Chapter 3

Glycan receptor targeted chitosan nanoparticles of gemcitabine

3 Glycan receptor targeted chitosan nanoparticles for targeted delivery of gemcitabine for lung cancer treatment.

3.1 Objective

The objective of this study was to optimize chitosan nanoparticles and develop novel glycan receptor targeted chitosan nanoparticles (CSN-NPs) conjugated with 5-N-acetyl-neuraminic acid (Neu5Ac) for gemcitabine (GMC) delivery in lung cancer cells. Targeted gemcitabine loaded 5-N-acetyl-neuraminic acid assembled chitosan nanoparticles (GMC-CSN-Neu5Ac-NPs) were formulated by ionotropic gelation process and evaluated for physicochemical and morphological properties and, *in vitro* and *in vivo* anticancer properties in A-549 cells and lung cancer mice model respectively. Results of gemcitabine loaded glycan receptor targeted chitosan NPs were compared to non-targeted and marketed gemcitabine (gemzer) injectable formulation for their therapeutic efficacy.

3.2 Plan of study

1) HPLC analytical and bioanalytical method development and validation
2) Experimental design for Optimization of chitosan nanoparticles
3) Formulation of gemcitabine encapsulated glycan receptor targeted and non-targeted nanoparticles
   i. Synthesis and purification of 5-N-acetyl-neuraminic acid conjugated chitosan (CSN-Neu5Ac).
   ii. Preparation of chitosan and CSN-Neu5Ac nanoparticles
4) Characterization of glycan receptor targeted nanoparticles
   i. ^{1}H-NMR, LC/MS and FTIR analysis of CSN-Neu5Ac conjugate
   ii. Morphological studies by SEM, TEM and AFM analysis
   iii. Measurement of particle size, PDI and zeta potential
   iv. Surface chemistry by X-ray photoelectron spectroscopy (XPS)
   v. Physical state of gemcitabine by X-ray diffraction (XRD) analysis
   vi. HPLC method for analysis of gemcitabine

5) Quantitative assessment of gemcitabine in nanoparticles as % entrapment efficiency
6) *In vitro* studies
   i. *In vitro* drug release studies at pH 5.5 and pH 7.4 buffer medium
   ii. *In vitro* cellular uptake and cytotoxicity studies on A-549 lung cancer cell line
7) *In vivo* studies
   i. Development (induction) of lung cancer in swiss albino mice
   ii. Tissue bio-distribution study
   iii. *In vivo* fluorescent imaging
   iv. Evaluation of toxicity in essential organs by histopathology examination
   v. *In vivo* anticancer efficacy in B[a]P induced lung cancer bearing mice.

3.3 Materials

Gemcitabine hydrochloride was provided by Neon Laboratories Pvt. Ltd., Mumbai India. Chitosan, degree of deacetylation minimum 90%, N-acetylneuraminic acid (Neu5AC), Formaldehyde solution, 1-Ethyl-3-(3-dimethylaminopropyl) carbodiimide (EDC), N-acetylneuraminic acid (NANA, Sialic acid), N-hydroxy succinimide (NHS) and Ehrlich reagent were purchased from Sisco Research Laboratories (SRL)-India. Dialysis membrane-70 (MW 14000 Dalton) was bought from HiMedia Laboratories Pvt. Ltd.-Mumbai, India. Acetic acid, sodium hydroxide (NaOH) pellets, HPLC quality water, acetonitrile and methanol were obtained from Merk Life Science Pvt.Ltd.-Mumbai, India. Clinical formulation GEMCIT used as drug control, was provided by *Getwell* Oncology Pvt. Ltd., Gurugram, India. The A-549 cell lines (human lung adenocarcinoma) were obtained from the National Centre for Cell Science (NCCS), Pune-India. Trypsin-EDTA, Dulbecco's modified Eagle's medium (DMEM), Fetal bovine serum (FBS), 3-(4,5-dimethyl thiazolyl-2-yl)-2,5-diphenyltetrazolium bromide (MTT) were purchased from Thermo Fisher Scientific-India. Sodium TPP, perchloric acid ($HClO_4$), penicillin, streptomycin, haematoxylin and eosin (H&E), Benzo-(a)-Pyrene, urethane,

thiopental sodium salt, coumarin 6 (C-6), 4′,6-diamidino-2-phenylindole (DAPI) and Dioctadecyl-3,3,3,3-Tetramethylindodicarbocyanine Perchlorate (DiD) were bought from Sigma-Aldrich.

3.4 Methods

3.4.1 HPLC analytical & bioanalytical method development and validation

The chromatographic separation of GMC were done on C18 column (shodex C18, 250x4.6mm, 5 µm) operated at 30°C using reversed-phase high-performance liquid chromatography (RP-HPLC) Agilent system using mobile phase composition of methanol: water in 20:80 ratio, injection volume was 20 0 µL, at a constant flow rate of 1 millilitre per minute (mL/min). The analytical samples of GMC were prepared in PBS (pH 7.4) & acetate buffer (pH 5.5) to obtain the required concentrations. The analysis was performed at a wavelength of 272 nm on PDA detector [224]. The method was validated for range and linearity, accuracy (recovery > 98% to < 101%) & precision (RSD: < 2%), specificity, selectivity & sensitivity [ICHQ2 (R1) 2005].

The bio-analytical method was developed in a similar manner. Plasma and tissues standards of GMC were made by spiking blank plasma and tissues samples with the primary working standard solution of GMC to obtain the required concentrations. GMC was extracted from plasma and tissues samples using chilled acetonitrile (precipitating agent) and vortexed for 5 min. The mixture was centrifuged at 12000 rpm for 15 min in a cooling centrifuge at 4 °C. Finally, clear supernatant was collected and concentration of GMC was estimated by HPLC. Samples were eluted using a mobile phase mixture of methanol: water in 20:80 ratio at a flow rate of 1 mL/min. The method was validated for range and linearity, accuracy (recovery > 98% to < 101%) & precision (RSD: < 2%), specificity, selectivity & sensitivity and percentage extraction recovery [ICHQ2 (R1) 2005].

3.4.2 Experimental design for Optimization of chitosan nanoparticles

The Design of Experiment (DoE) was done by Design Expert software through Box-Behnken surface analysis. DoE works based on variables to optimize the results and predicts the influence of individual and combined effects of factors. DoE was comprehensively used in the application of Quality by design (QbD) in the study.

In a previous study conducted by Arujana et al. (2021), the selected levels ranged from 0.5 to 1 % with respect to CSN and from 0.5 to 2 % for TPP [225]. The low and high levels of CSN and TPP were chosen based on our preliminary experiments of the effects of these factors (CSN and TPP) on particle size, zeta potential, PDI and EE%. In our study, below 1 mg/ml CSN and 0.25 mg/ml TPP, NPs were not efficiently formed due to the inappropriate concentration ratio of CSN and TPP necessary for crosslinking. Additionally, concentrations ratios above 2 mg/ml CSN and above 0.75 mg/ml TPP led to non-uniform NPs with larger particle size and higher PDI. Based on our preliminary study, broader ranges were studied. The medium levels of the different factors were automatically generated by the software based on the selected low and high levels.

We utilised Box-Behnken design (BBD) with three factor and three levels to examine the relationship between the factors (independent variables): concentration of CSN (factor A), the concentration of TPP (factor B) and the volume of TPP (factor C) and the associated response (dependent variables). The response variables were particle size, PDI, zeta potential and entrapment efficiency. Based on the preliminary assessment, the range of independent variable was decided. They were investigated for three distinct levels, namely low (-1) middle (0) and high (+1) **(Table 3.1).** Design-Expert (Stat-Ease, Inc. 2021 East Hennepin Ave., suite 480 Design Expert Version 7.0.0, Minneapolis, MN 55413) designed an experimental matrix with 17-runs with five central points. The best fit statistical model was chosen based on measures like correlation coefficients (R^2), adjusted R^2, predicted R^2, coefficient of variation (CV) and lack of fit. For statistical validation one-way analysis of variance (ANOVA) was used.

Table 3.1 Design of experiment by Box Behnken design (alongwith their levels and limitations applied).

Factors/Responses		Levels		
		Low level (-1)	**Medium level (0)**	**High level (+1)**
Independent Variables (Factors)	Chitosan (mg/ml)	1	1.5	2
	TPP (mg/ml)	0.25	0.5	0.75
	Volume of TPP (ml)	1	4.5	8
Dependent Variables	Particle size (nm)		Minimum	
	PDI		Minimum	

(Responses)	Zeta potential (mV)	Maximum
	Entrapment Efficiency (%EE)	Maximum

3.4.3 Formulation of GMC encapsulated non-targeted and targeted nanoparticles

3.4.3.1 Synthesis and purification of Neu5Ac conjugated chitosan

Neu5Ac was coupled with chitosan utilising EDC chemistry, with slight changes to the previously described method [226]. Based on the stoichiometric calculations, briefly 81.04 mg of Neu5Ac and 61.01 mg of 1-(3-dimethyl aminopropyl)-3-ethyl carbodiimide hydrochloride (EDC) were dissolved in 10 mL of distilled water, after 10-15 minutes of stirring, 60.31 mg of *N*-hydroxysuccinimide (NHS) was added to above solution. The reaction mixture was stirred 1-2 hours at room temperature to activate carboxyl groups (EDC reacts with carboxylic acid group of Neu5Ac to produce an active O-acylisourea unstable intermediate that can be easily displaced by nucleophilic attack from primary amino groups in the reaction mixture) and form an intermediate of semistable amine reactive NHS ester. Chitosan solution (0.8%) was made by dissolving 200 mg of chitosan in acetate buffer (pH 4.7), then it was added to Neu5Ac solution and stirred overnight. The solution was then added to a dialysis membrane and dialyzed using distilled water for 24 hours to eliminate the unreacted Neu5Ac and EDC. The resulting solution was filtered through membrane filter to purify the conjugate. The resulting filtrate was freeze-dried for up to 10-12 hours to produce a dry powder. The chemical synthesis of 5-N-acetyl-neuraminic acid-chitosan (CSN-Neu5Ac) conjugate has been depicted in **Figure 3.1**.

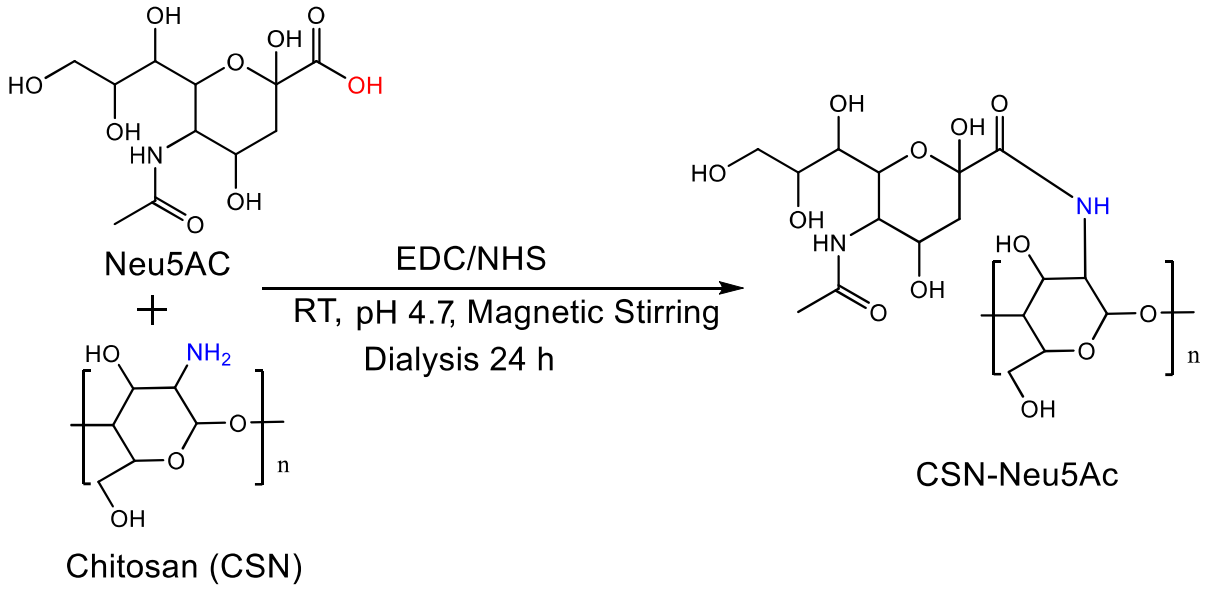

Figure 3.1 Schematic representation for the chemical synthesis of CSN-Neu5AC conjugate.

3.4.3.2 Method of preparation of chitosan nanoparticles and 5-N-acetyl-neuraminic acid conjugated chitosan nanoparticles

GMC loaded CSN-NPs were formulated by ionic crosslinking process using aqueous solution of Na-TPP. To the aqueous acetic acid solution (0.2 % v/v) of CSN and CSN-Neu5Ac (1 mg/ml) each, aqueous solution of GMC (5 mg/ml) was added under stirring **(Table 3.2)** for 2 h. Then, 4 ml of aqueous solution of Na-TPP (0.5 mg/ml) was added drop-wise to each of CSN-GMC and CSN-Neu5Ac-GMC solution with 4-5 h of continuous stirring for the formation of GMC-CSN-NPs and GMC-CSN-Neu5Ac-NPs (**Figure 3.2 A, B).** Thereafter, NPs were separated by centrifugation at 15000 rpm for 10 min to eliminate entrapped GMC and TPP, followed by washing with distilled water and re-suspension in phosphate buffer saline (PBS).

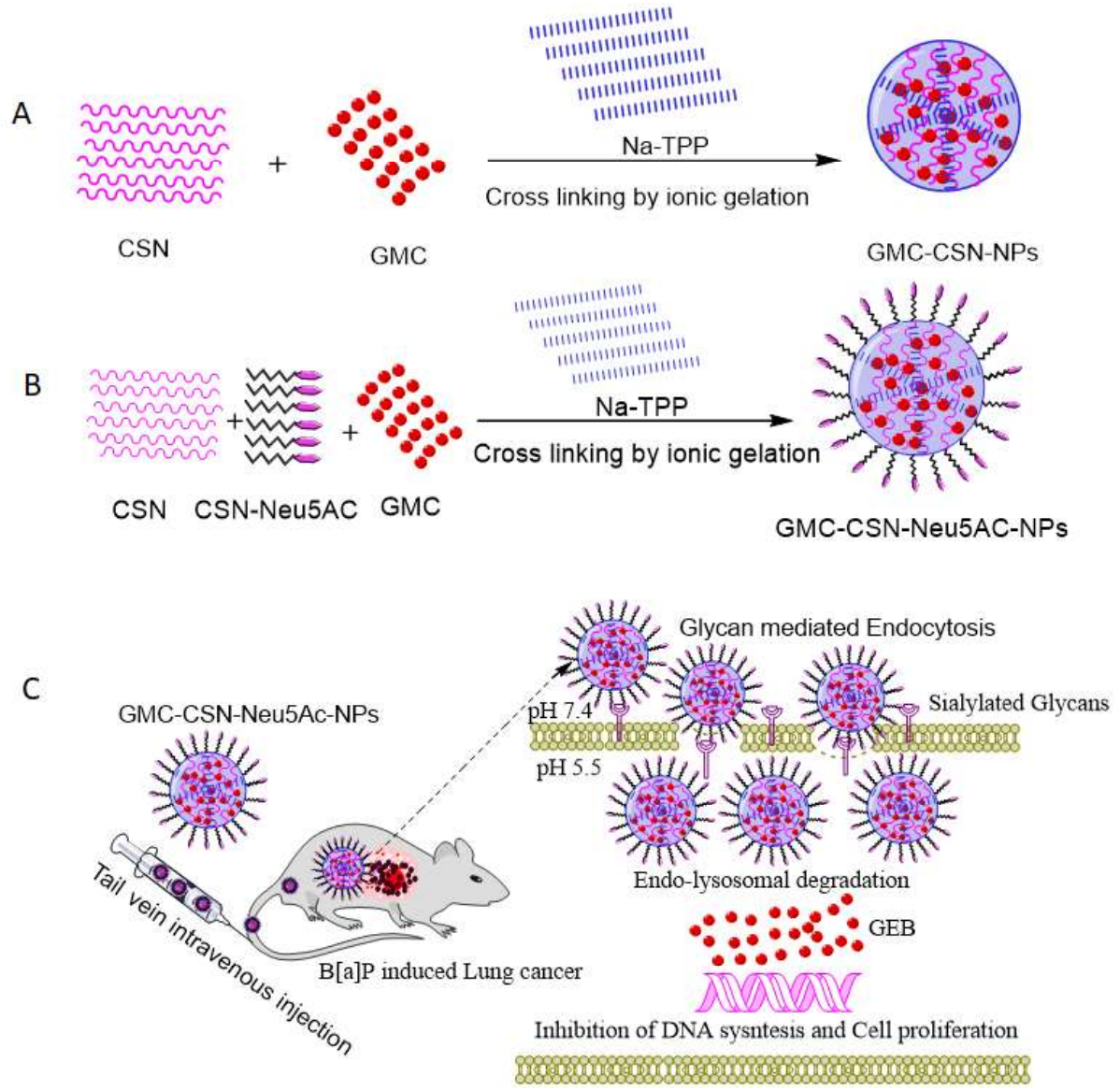

Figure 3.2 A. Preparation of gemcitabine encapsulated chitosan nanoparticles (GMC-CSN-NPs); B. Preparation of gemcitabine encapsulated Neu5Ac conjugated chitosan nanoparticles (GMC-CSN-Neu5Ac-NPs); C. Proposed mechanism of therapeutic action of glycan receptor targeted NPs (GMC-CSN-Neu5Ac-NPs) via inhibition of DNA synthesis and cell proliferation in lung cancer mice model.

For *in vivo* fluorescent bio-imaging, DiD was tagged to GMC-CSN-NPs and GMC-CSN-Neu5Ac-NPs, by adding 20 µL of DiD (1 mg/ml in DMSO) to 1 ml of each of GMC-CSN-NPs and GMC-CSN-Neu5Ac-NPs suspension in PBS, with stirring for 24 h in dark. Further, resultant NPs suspension was subjected to centrifugation followed by removal of supernatant and washing of pellet, and re-dispersion in PBS, which was then used for bio-imaging studies.

Table 3.2 Formulation of gemcitabine loaded non-targeted and targeted chitosan nanoparticles.

Nanoformulations	CSN-Neu5Ac (mg)	CSN (mg)	GMC (mg)	DiD (mg)	Na-TPP (mg)
GMC-CSN-NPs	0	10	10	0	2
GMC-CSN-Neu5Ac-NPs	5	5	10	0	2
DiD-GMC-CSN-NPs	0	10	10	0.02	2
DiD-GMC-CSN-Neu5Ac-NPs	5	5	10	0.02	2

Note: GMC-CSN-NPs: GMC encapsulated chitosan NPs; GMC-CSN-Neu5Ac-NPs: GMC encapsulated Neu5Ac conjugated chitosan NPs; DiD-GMC-CSN-NPs: GMC encapsulated DiD incubated chitosan NPs; and DiD-GMC-CSN- Neu5Ac-NPs: GMC encapsulated DiD incubated Neu5Ac conjugated chitosan NPs.

3.4.4 Characterization of chitosan nanoparticles and 5-N-acetyl-neuraminic-acid conjugated chitosan nanoparticles

3.4.4.1 ^{1}H-NMR, LC/MS and FTIR analysis of CSN-Neu5Ac conjugate

Proton nuclear magnetic resonance (^{1}H-NMR), mass spectrometry (LC/MS) and Fourier transform infrared spectroscopy (FTIR) were used to evaluate the CSN-Neu5Ac conjugate in order to validate the conjugation as well as the purity of conjugate.

For ^{1}H-NMR, 1 mg of pure CSN-Neu5Ac conjugate was dissolved in 600 microliter (μL) each of deuterated dimethyl sulfoxide (DMSO) and D2O and analysed on 500 MHz ^{1}H-NMR spectrometer (Bruker BioSpin International AG). For the mass spectrometry (LC/MS) analysis, 1 milligram per millilitre (mg/mL) primary stock solution of the CSN-Neu5Ac conjugate was made in methanol and further diluted 1000 times with methanol before characterisation on liquid chromatography (LC) coupled with high resolution quadrupole Time of flight (QTOF) mass spectrometry (MS) system (Sciex, X500B QTOR, SN: DM221391904, SINGAPORE) obtaining the conjugate's mass spectra while working in positive ion mode. FTIR spectra were recorded on an infrared detector (THERMO Electron Scientific). Approximately 1 mg each dry CSN, Neu5Ac and CSN-Neu5Ac powder were mixed with potassium bromide (KBr) and then pressed to a plate for measurement.

3.4.4.2 Physicochemical characterization of nanoparticles for morphological studies, particle size, PDI, zeta potential, XPS and XRD

To characterize the shape, size and surface morphology of CSN-NPs, scanning electron microscopy (SEM), transmission electron microscopy (TEM) and atomic force microscopy (AFM) were performed [227,228]. For SEM analysis, a drop of NPs suspension diluted with ultrapure water was applied on coverslips and dried for 24 h at 45°C to obtain uniform dried film of NPs. These NPs were coated with carbon, and observed under SEM (MA15/18, CARL ZEISS MICROSCOPY LTD), for TEM examination, a single drop of aqueous solution of respective NPs was positioned on the copper TEM grid with carbon coating and air dried overnight at room temperature before examination in TEM (FEI Tecnai G2 20-TWIN). For AFM study, NPs were diluted with ultrapure water and sonicated, a drop of prepared sample was casted on a glass slide and air dried overnight and then examined by AFM (NT-MDT Service & Logistics Ltd. Moscow, Russia). 2-D and 3-D AFM images of NPs were processed using NOVA, NT-MDT software.

The hydrodynamic particle size distribution, polydispersity index (PDI) and zeta potential were determined by zetasizer (Malvern ZetasizerNanoseries) at 25°C by dynamic light scattering method [229].The nanoformulations were appropriately diluted before analysis.

To confirm the coating of Neu5Ac on surface of CSN-NPs and atomic composition on surface of nanoformulations, XPS (X-ray photoelectron spectroscopy) (K-Alpha, Thermo Fisher Scientific) analysis was carried out at binding energies in the range of 100-600 eV[230]. The samples were fixed by drop casting process by introducing a drop of NP on a glass slide and air dried for 24 h before XPS examination.

Physical state of the NPs was evaluated by XRD analysis [231]. XRD examination of GMC, GMC-CSN-NPs, GMC-CSN-Neu5Ac-NPs, along with CSN, Neu5Ac, and CSN-Neu5Ac conjugates was accomplished by bench top X-ray diffractometer (Rigaku Americas Corporation).

3.4.5 HPLC method for analysis of GMC

The reverse-phase high-performance liquid chromatography (RP-HPLC, Agilent, USA) separations were performed on C18 column (shodex C18, 250x4.6mm, 5um), using PDA detector at 30°C. The elutions were performed using methanol: water (20:80) mobile phase at a flow rate of 1 ml/min and wave length of 272 nm [224].

3.4.6 Entrapment efficiency of gemcitabine and *in vitro* drug release study

The amount of GMC entrapped in the CSN-NPs was estimated by HPLC analysis. Concisely, 1 ml of CSN-NPs were placed for centrifugation at 10,000 rpm for 30 min. The supernatant was diluted with HPLC grade ultrapure water. Afterward dilution, approximately 800 µL sample was used for HPLC analysis [232]. The total amount of GMC in CSN-NPs was determined from the peak area obtained from the standard curve of GMC.

The drug entrapment efficiency (%EE) of CSN-NPs was estimated by the formula given below.

$$\%EE = \frac{Total\ amount\ of\ GMC\ added\ in\ Formulation - Amount\ of\ free\ drug}{Total\ amount\ of\ GMC\ added\ in\ formulation} * 100$$

The dialysis membrane diffusion method was used to examine the amount of GMC released from CSN-NPs. The nanosuspension corresponding to 0.6 mg/ml of the GMC, were placed in a dialysis bag. The bag was closed from both the ends and immersed in 30 ml of acetate-buffer (pH 5.5) and phosphate-buffered saline (pH 7.4) medium separately at 37 ± 0.5°C with constant magnetic stirring at 120 rpm [233]. Specifically, 1 ml of the release medium was withdrawn at predefined time points and replaced with equal volume of fresh buffer media. All samples were filtered through a 0.22 micron syringe filter, and amount of GMC in samples was measured by HPLC method. The data was plotted graphically between cumulative percent drug release and time interval.

3.4.7 Cellular uptake

In order to formulate coumarin-6 (C6) tagged drug and nanoformulations, coumarin-6 (0.5 mg/ml) was dissolved in ethanol, and 1 ml of that solution was subsequently subjected to incubation with 1 ml

of each of pure drug (GMC), GMC-CSN-NPs, and GMC-CSN-Neu5Ac-NPs. Confocal microscopy was used to examine the cellular uptake study of C6-GMC, C6-GMC-CSN-NPs, and C6-GMC-CSN-Neu5Ac-NPs on A-549 cells. The cells were seeded on sterilized coverslips in 6-well plates at a density of 5×10^4 cells per well, and allowed to grow for 24 h in DMEM medium incubated with C6 labelled GMC control, GMC-CSN-NPs and GMC-CSN-Neu5Ac-NPs (equivalent to 50 μg/ml of GMC) respectively. Following incubation, the A-549 cells were thoroughly cleaned with PBS and fixed for 5-10 min in 4% paraformaldehyde solution. The nuclei of cells were stained with 4′, 6-diamidino-2-phenylindole (DAPI) for further 15-20 min. The cells were afterward washed with PBS and examined under a Zeiss LSM900 confocal laser scanning microscope (Zeiss, Jena, Germany) by setting the blue and green signals for DAPI and C6 at excitation wavelength of 405 and 488 nm, respectively. The Zeiss Zen 3.6 blue edition software was used for analysing fluorescent images and the image-J software was used to evaluate the green fluorescence images of all C6 tagged formulations [234]. The overall area covered by C6 in A-549 cells, depicted by green channel, confirmed the cellular uptake of formulations.

3.4.8 Cytotoxicity study

In vitro cytotoxicity of the GMC-CSN-NPs and GMC-CSN-Neu5Ac-NPs was compared with GMC control evaluated on A549 lung cancer cell lines. The A549 cells were inoculated with 3×10^4 viable cells/well in 96-well plates in 200 μL DMEM medium and allowed to adhere and grow at 37 °C, 5% CO_2 for 24 h. In DMEM media, the cells were sequentially treated for 24 h with GMC control and corresponding GMC loaded CSN-NPs at doses ranging from 0.01 to 100 μg/ml of GMC. After that, a 10 μL MTT mixture (5 mg/ml in PBS) was poured in all wells and treated for 4 h to form purple formazan crystals. Subsequently, the left-over supernatant was then replaced with 100 μL DMSO, and the resulting solution was shaken for an additional 10 min to dissolve the formazan crystals. Next, using a microplate reader (Synergy H1), the absorbance of solution was recorded at 570 nm [235]. The IC_{50} was measured by GraphPad Prism Software (GraphPad Prism version 5.0, California). The percentage of viable cells was estimated by using the following equation:

$$Cell\ Viability\ (\%) = \frac{Absorbance\ of\ treated\ cells}{Absorbance\ of\ control\ cells} * 100$$

3.4.9 Animal Ethics

The animal experiments were conducted in accordance with the guidelines established by the Institutional Animal Ethics Committee. These standards pertain to the regulation and oversight of experimental animals and are governed by the Animal Protection and Welfare Section of the Government of India, located in New Delhi. The specific reference number for compliance with these regulations is 2123/GO/Re/S/21/CPCSEA.

3.4.10 Development (induction) of Lung cancer

Lung cancer was induced chemically in male swiss albino mice weighing between 20-25 g, via peroral delivery of 50 mg/kg of Benzo [a] pyrene (B[a]P) dispersed in olive oil to mice two times in a week (1^{st} and 4^{th} day) up to 4 consecutive weeks, and the induction of the cancerous lesions was confirmed by histopathological examination [236].

3.4.11 Tissue bio-distribution study

Lung cancer-bearing swiss albino mice were divided into three groups: drug control (pure drug GMC) solution [Group I], GMC-CSN-NPs [Group II] and GMC-CSN-Neu5Ac-NPs [Group III] administered with GMC at a dose equivalent to 10 mg/kg body weight intravenously through lateral tail vein. Three animals from each group were sacrificed at predetermined time points (2, 12 and 24 h) and their lungs, heart, liver, spleen, and kidneys were surgically extracted and washed with saline [237]. The tissues were cut into small pieces and 1.0 g of tissue samples was incubated with 2.0 ml of PBS solution and subjected to high speed homogenization for 2 min at 4°C. The homogenate was then centrifuged at 12,000 rpm for 10 min. Thereafter, acetonitrile was added to supernatant to precipitate un-wanted proteins and centrifuged again at 12,000 rpm for 10 min. Finally, clear supernatant was collected and concentration of GMC was estimated by HPLC.

3.4.12 *In vivo* fluorescent imaging

The lung cancer bearing swiss albino mice were divided into three groups. The mice were anaesthetized by intra-peritoneal injection of thiopentone sodium at a dose of 0.2 mg/kg. Group A was injected with free DiD dye, while Group B and Group C were injected with DiD loaded NPs: DiD-GMC-CSN-NPs and DiD-GMC-CSN-Neu5Ac-NPs respectively through tail vein. Bio-images were captured at 1, 4, 12 and 24 h post administration using *in vivo* imaging system (PHOTONIMAGER OPTIMA, Biospace Lab, France) by adjusting excitation/emission maxima at 637/672 nm in near infrared region of DiD dye.

3.4.13 Histopathology

The toxicity of non-targeted (GMC-CSN-NPs) and targeted (GMC-CSN-Neu5Ac-NPs) NPs was evaluated by histopathological examination. The saline control, GMC control, non-targeted and targeted formulations were administered intravenously to individual groups of swiss albino mice via tail vein two times a week (1^{st} and 4^{th} day) up to 4 consecutive weeks. After 28 days of treatment animals were euthanized and essential organs (heart, lungs, liver, and kidneys) were removed and cleaned with sterile saline. The collected organs were placed in 10%v/v formalin solution and embedded with paraffin and sectioned using microtome. The paraffin sections of 5µm thickness were fixed on separate glass slides and stained with haematoxylin and eosin (H&E) for assessment of tissue physiology under optical microscope [238].

3.4.14 *In vivo* anti-cancer efficacy

The experimental animals were distributed into five groups with every group consisting of six swiss albino mice: Group I (negative control) was administered olive oil orally twice a week throughout the experimental period. Group II (model control) was delivered (B[a]P) (50 mg/kg bodyweight dispersed in olive oil) orally twice a week (1^{st} and 4^{th} day) up to 4 weeks. Group III (drug control), IV (non-targeted NPs) and V (targeted NPs) were administered with GMC control, GMC-CSN-NPs and GMC-CSN-Neu5Ac-NPs (10 mg GMC/kg bodyweight) respectively via intravenous injection in tail vein twice a week in between week 4 and week 8 post-B(a)P therapy. Throughout the study, health

condition of the mice was monitored daily during the trial, and their body weights were recorded weekly. Kaplan-Meier graphical model were used to analyse the survival data in terms of percentage of survival. All the surviving mice were anesthetized after 16 weeks using urethane (2 g/kg bodyweight, intraperitoneally) and then sacrificed. Thereafter , lungs from all the groups were removed, fixed with 10% formalin, encased in paraffin blocks, sectioned (5µm thick), and fixed on glass slides. Haematoxylin and eosin (H&E) staining was used to observe the tissue sections using an optical microscope [239,240]. The optical images were analysed for histopathological changes, and number of cells and; their extent of proliferation was evaluated using Image J software [234].

3.4.15 Statistical Data analysis

The data was analysed statistically using one-way analysis of variance (ANOVA) and Tukey-Kramer multiple comparison post-test, and results have been presented as mean ±SD (GraphPad Software, California). Statistically significant differences have been denoted as *(* $p < 0.05$)*, *(** $p < 0.01$)* and *(*** $p < 0.001$),* respectively. Values that were non-significant *(ns)* have been represented as *($p > 0.05$).*

3.5 Results and Discussion

3.5.1 Analytical and bio-analytical HPLC method validation

3.5.1.1 Range and Linearity

The average area under curve of GMC plotted against their respective concentrations in PBS (pH7.4), Acetate buffer (pH 5.5) for *in-vitro* samples and in plasma and tissues for *in-vivo* samples were presented in **Figure 3.3.** A linear relationship was found between the selected concentrations of GMC at PBS (pH7.4) & Acetate buffer (pH 5.5) (1000 ng/mL to 10000 µg/mL) and the chromatographic area (at 272 nm) with correlation coefficients (r^2) 0.9973, 0.9987 respectively. Similarly, a linear relationship was found in plasma and tissues samples (lungs, liver, heart, spleen & kidney) between the used concentrations of GMC (100 ng/mL to 6000 ng/mL for plasma and 10-2000 ng/mL for tissues) and the corresponding chromatographic area (at 272 nm) with correlation coefficients (r^2) 0.9957, 0.9908, 0. 988, 0.991, 0.9917 & 0.9873 respectively. The high correlation coefficient values

(r^2 = 0.99) for both *in-vitro* & *in-vivo* samples of the fitted model indicate a strong relationship among the variables and confirmed their suitability for the further analysis **(Table 3.3)**.

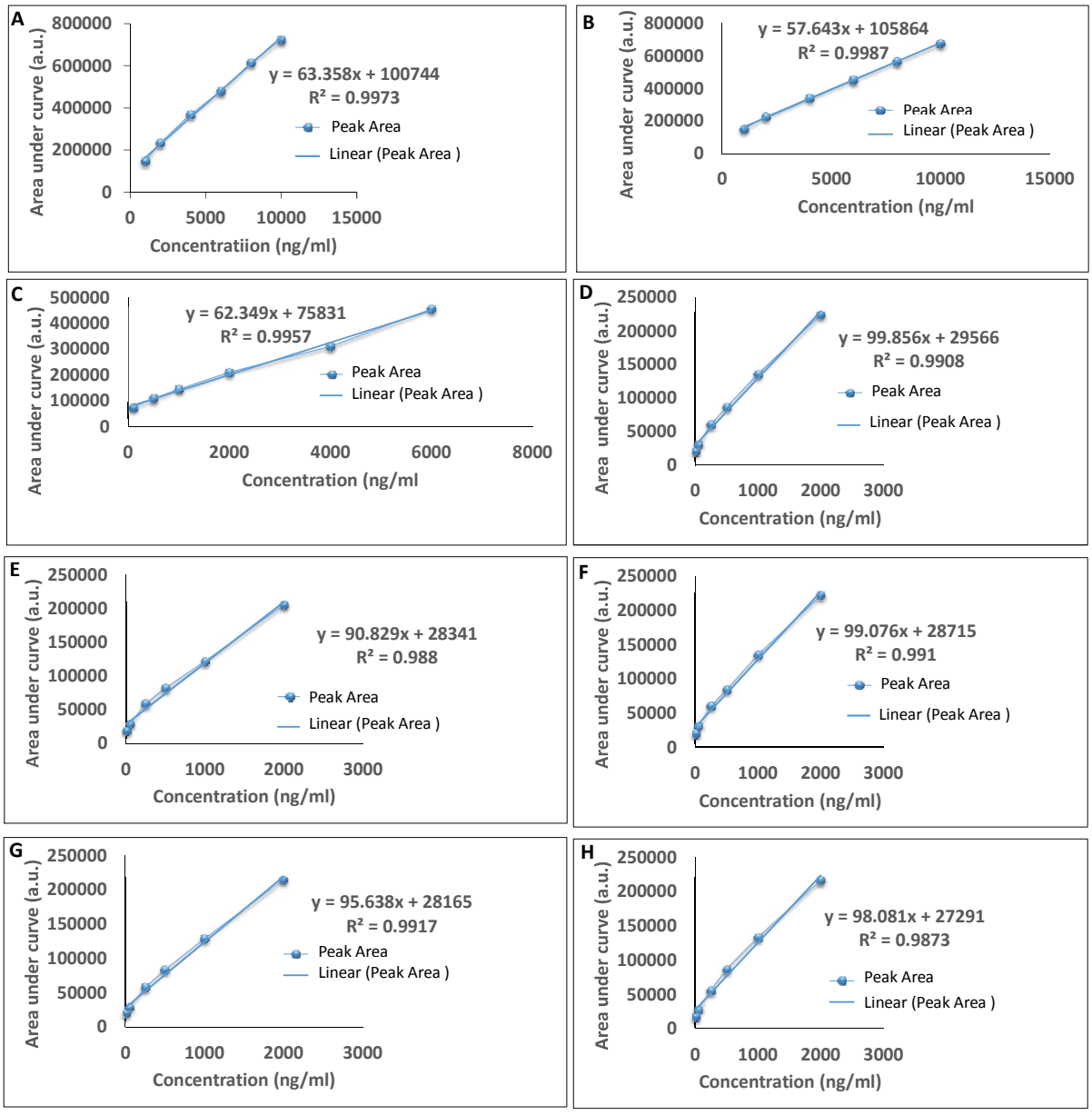

Figure 3.3 Calibration curves of GMC in (A) PBS pH 7.4 (B) acetate buffer pH 5.5 (C) plasma & in tissues (D) lung (E) liver (F) heart (G) spleen (H) kidney at wavelength 272 nm.

Table 3.3 HPLC validation parameters for determination of GMC in analytical & bioanalytical samples.

Parameters	pH 7.4	pH 5.5	Plasma	Lungs	Liver	Heart	Spleen	Kidney
Wavelength (nm)	272	272	272	272	272	272	272	272
Retention	4.0	4.0	4.2	4.4	4.4	4.3	4.3	4.3

time (min.)								
Slop	63.358	57.643	62.349	99.856	90.829	99.076	95.638	98.081
Intercept	100744	105864	75831	29566	28341	28715	28165	27291
Correlation coefficient (R^2)	0.9973	0.9987	0.9957	0.9908	0.988	0.991	0.9917	0.9873
Range (ng/mL)	1000-10000	1000-10000	100-6000	10-2000	10-2000	10-2000	10-2000	10-2000
LOD (ng/mL)	256.63	152.38	71.67	6.56	4.13	6.89	5.73	6.44
LOQ (ng/mL)	478.50	586.35	90.86	57.45	45.50	60.27	60.80	62.99

3.5.1.2 Accuracy and precision

The closeness of theoretical (concentrations of drug added) and experimental values (concentrations of drug recovered) indicates the accuracy of the analytical method. Precision represents the closeness among a series of readings obtained from multiple sampling of the same homogeneous sample under specified analytical conditions. These are calculated by analysing standard samples at 3 different concentrations in triplicate within the calibration range.

The accuracy of the method in terms of % drug recovered was found to be 99 to 101 % for GMC indicating acceptable limit of the method. The interday and intraday precision (RSD value) was found to be <2%, indicating repeatability of the developed HPLC method **(Table 3.4)**.

Table 3.4 Accuracy & precision (Intra-day and inter-day precision) studies of the developed analytical & bio analytical HPLC method.

Samples	Standard Sample (ng/mL)	Level of recovery	Drug added (ng/mL)	Drug recovered (ng/mL) (mean± S.D)	% Drug recovered	Precision Intraday	Interday
pH 7.4	1000	80%	800	801.80±0.56	100.22	1.00	1.95
		100%	1000	991.74±0.15	99.17	1.34	2.08
		120%	1200	1198.17±0.28	99.84	1.97	1.59
pH 5.5	1000	80%	800	811.62±0.15	101.45	1.79	1.96
		100%	1000	1008.98±0.18	100.89	1.21	0.68
		120%	1200	1197.10±0.17	99.75	1.33	1.99
Plasma	1000	80%	800	798.91±0.19	99.86	1.93	1.78

		100%	1000	997.34±0.56	99.73	1.32	1.38
		120%	1200	1198.19±0.81	99.84	1.48	1.49
Lungs	1000	80%	800	802.99±0.56	100.37	1.92	1.40
		100%	1000	998.63±0.44	99.96	1.93	1.97
		120%	1200	1198.68±0.24	99.89	1.12	1.98
Liver	1000	80%	800	797.95±0.34	99.74	1.16	1.91
		100%	1000	999.18±0.35	99.81	1.57	2.06
		120%	1200	1198.07±0.65	99.83	1.75	1.66
Heart	1000	80%	800	801.17±0.31	100.14	1.27	1.98
		100%	1000	999.23±0.28	99.92	1.86	1.83
		120%	1200	1199.19±0.29	99.93	1.90	1.89
Spleen	1000	80%	800	798.13±0.56	99.76	1.76	1.98
		100%	1000	999.25±0.21	99.81	1.78	1.99
		120%	1200	1198.05±0.78	99.83	1.83	1.93
Kidney	1000	80%	800	799.98±0.76	99.99	1.78	1.89
		100%	1000	998.56±0.55	99.85	1.57	1.94
		120%	1200	1198.37±0.57	99.86	1.89	1.58

3.5.1.3 Specificity, selectivity and sensitivity

The developed method was found to be specific and selective. The developed method showed no interfering peaks **(Figure 3.4)** of excipients at respective retention time of GMC indicating specificity of the developed method.

To determine the sensitivity, limit of detection (LOD) and limit of quantitation (LOQ) were calculated. LOD refers to the minimum concentration of an analyte in a sample that can be identified, although not necessarily precisely quantified. On the other hand, the limit of quantitation (LOQ) is the minimum concentration of an analyte in a sample that can be accurately and precisely quantified. The determination of LOD and LOQ for the analytical method was carried out in accordance with established protocols and using specific equations [ICHQ2 (R1)].

LOD = 3.3 SD/Slop

*L*OQ=10 SD/Slop

The LOD and LOQ values for the determination of GMC **(Table 3.3)** were found to be 256.63 & 478.50 ng/mL (pH 7.4), 152.38 & 586.35 ng/mL (pH 5.5) for analytical samples. Similarly, the LOD and LOQ values for bio analytical samples of GMC were 71.67 & 90.86 ng/mL (plasma), 6.56 &

57.45 ng/mL (lung), 4.13 & 45.50 ng/mL (liver), 6.89 & 60.27 ng/mL (heart), 5.73 & 60.80 ng/mL (spleen) and 6.44 & 62.99 ng/mL (kidney) respectively. The lower values of LOD and LOQ indicated the sensitivity of the developed HPLC method for determination of GMC. During analysis and preparation of calibration curves, the curves was prepared from LOQ onwards.

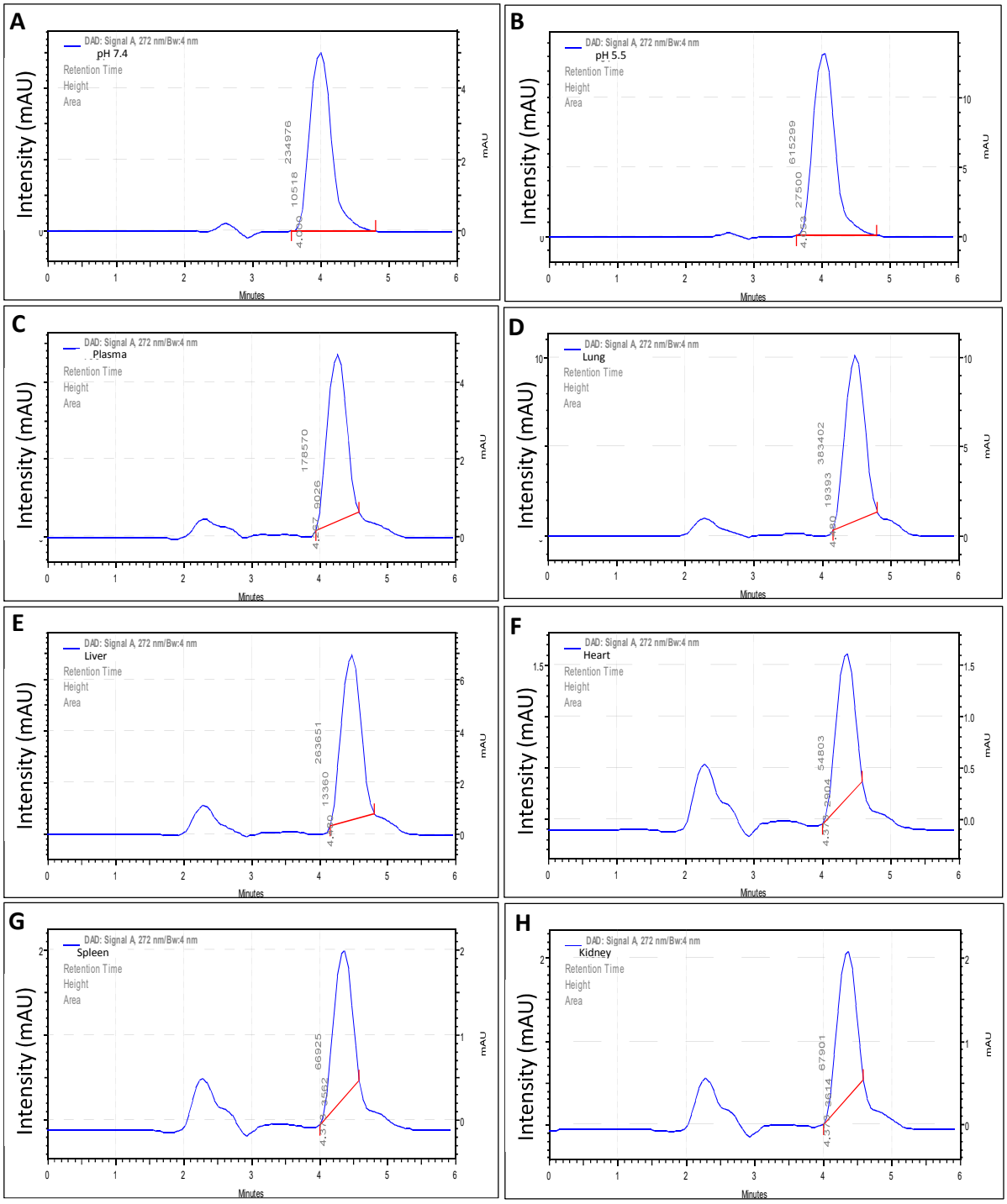

Figure 3.4 Selectivity of GMC in (A) PBS pH 7.4 (B) acetate buffer pH 5.5 (C) plasma & in tissues (D) lung (E) liver (F) heart (G) spleen (H) kidney at wavelength 272 nm.

3.5.1.4 Percentage extraction recovery (%ER)

The %ER represents the extraction ability of the used organic solvent in the developed method for extraction of analyte. As per the FDA guideline, the %ER need not be 100%, but the extent of the recovery of an analyte should be reproducible and consistent. The mean %ER of GMC from the plasma and tissue samples (Lungs, Liver, Heart, Spleen & Kidney) with respect to GMC in PBS 7.4 were found to be 95.98±1.02 %, 92.69±1.53 %, 91.96±1.48 %, 91.99±0.23 %, 93.48±0.38 % & 94.27±0.25 % respectively **(Table 3.5**).The consistent and high % ER values demonstrated the suitability of the used method for the extraction of analytes from plasma and tissue samples and their quantification through the developed HPLC method.

Table 3.5 Percent extraction recovery (%ER) of GMC through the developed HPLC method (n = 3).

Sample	GMC spiked concentration (ng/mL)	%ER ±SD (n=3)
Plasma	1000	95.98±1.02
Lungs	1000	92.69±1.53
Liver	1000	91.96±1.48
Heart	1000	91.99±0.23
Spleen	1000	93.48±0.38
Kidney	1000	94.27±0.25

3.5.2 Design of experiments (DOE) for optimization of chitosan nanoparticles

For the development of an effective formulation, the prepared gemcitabine loaded chitosan nanoparticles were optimised by DOE utilising response surface analysis by the Box-Behnken design (BBD). BBD is an efficient approach for exploring multiple variables at different levels with lesser number of trial runs. In the proposed work, we have selected concentration (in mg/ml) of CSN, TPP, and volume of TPP (in ml) as factor variables at low, medium, and high levels. Based on the experimental design 17 distinct runs with varying quantities of CSN, TPP, and volume of TPP were predicted for preparing of formulations.

Table 3.6 Experiential responses of nanoformulations as per Box-Behnken design.

	Independent variables (Factors)			Dependent variables (Responses)			
Runs	**Chitosan (mg/ml)**	**TPP (mg/ml)**	**Volume of TPP solution (ml)**	**Particle size (nm)**	**PDI**	**Zeta potential (mV)**	**Entrapment Efficiency (%EE)**
1	1.5	0.5	4.5	339.4	0.233	29.5	65.37

2	**1**	**0.5**	**8.00**	**149.3**	**0.260**	**51.7**	**70.21**
3	2	0.5	1.00	366.4	0.265	41.9	43.67
4	1.5	0.25	8.00	289	0.411	45.3	67.7
5	2	0.25	4.5	289	0.372	36.1	62.9
6	1.5	0.5	4.5	331.7	0.272	29.3	61.8
7	1	0.5	1.00	343.2	0.449	24.4	40.4
8	1.5	0.25	1.00	351.1	0.5	44.3	50.2
9	1.5	0.75	8.00	331.3	0.338	42.8	67.9
10	2	0.75	4.5	240.1	0.331	23.7	49.3
11	1	0.25	4.5	301.9	0.479	28.6	58.2
12	1.5	0.75	1.00	441.5	0.343	29.5	29.4
13	2	0.5	8.00	276.1	0.435	29.1	61.8
14	1.5	0.5	4.5	330.4	0.270	33.1	50.2
15	1	0.75	4.5	311.8	0.276	37.2	44.3
16	1	0.75	1.00	402.1	0.409	25.2	20.3
17	2	0.50	4.50	308.9	0.355	22.1	52.1

***** Bold values indicate optimized values predicted by Design Expert software.

3.5.2.1 Analysis of Response

All of the obtained responses for the 17 formulations **(Table 3.6)** were sequentially fitted to 1st order, 2nd order, and quadratic models. The particle size, PDI, zeta potential and %EE of the prepared 17 batches ranged from 149.30 nm to 441.50 nm, 0.233 to 0.500, 22.10 mV to 51.70 mV and 20.30 % to 70.21 % respectively. The 2D and 3D surface response plots for various factors like particle size, PDI, zeta potential and %EE have been shown in **Figure 3.5, 3.6, 3.7 and 3.8.** All experimental responses were fitted to a quadratic (for particle size, PDI, zeta potential) and 2FI (%EE) model and a full model polynomial equation was generated. The following equations were generated in terms of coded factors; concentration of chitosan (A), concentration of TPP (B), volume of TPP (C):

Particle size = 257.28+97.61*A+42.50*B-58.19*C+6.81*A*B+8.51*A*C-16.45*B*C-16.41*A^2+17.07*B^2-4.89*C^2

PDI = 0.36-0.083*A-5.225E-004*B-0.078*C+0.031*A*B+0.029*A*C+9.100E003*B*C+0.020*A^2+0.068* B^2+0.010*C^2

Zeta Potential = 29.56 +2.28*A+10.68* B+8.64*C-3.80*A*B-3.28*A*C+1.39*B*C-1.13*A^2+2.73* B^2+1.49*C^2

Entrapment Efficencey = 38.11+1.89*A-9.65* B+11.11* C+0.65*A* B-1.19*A*C+2.59* B*C

3.5.2.2 Correlation coefficient

The correlation coefficient (R^2) for particle size, PDI, zeta potential and %EE efficiency showed an acceptable fit. It was found that the predicted R^2 value was pretty close to the adjusted R^2, i.e., the variation was smaller than 0.2. The observed R^2 value for particle size was 0.9451, while the predicted R^2 value was 0.8216. Subsequently, for PDI observed R^2 was 0.8797, against the predicted R^2 of 0.7642. Lastly, the observed R^2 of zeta potential was 0.8956, v/s predicted R^2 of 0.7048.

3.5.2.3 Optimization by desirability approach

The quantitative optimization method based on desirability approach was applied for optimization of gemcitabine loaded chitosan nanoparticles with goal of obtaining minimum particle size and PDI and maximum zeta potential and entrapment efficiency. The levels of variables that produce the best response were identified along with overall desirability of predicted factors which were concentration of chitosan 1 mg/ml, concentration of TPP 0.5 mg/ml and volume of TPP 8 ml. The predicted values of response were particle size 152.11 nm, PDI 0.236, zeta potential 54.35 and entrapment efficiency 70.52% with overall desirability of 0.995. The optimized formulation prepared with the predicted factors exhibited particle size of 149.3 nm; PDI 0.260; zeta potential 51.7 mV and; entrapment efficiency 70.21% which were very close to predicted response.

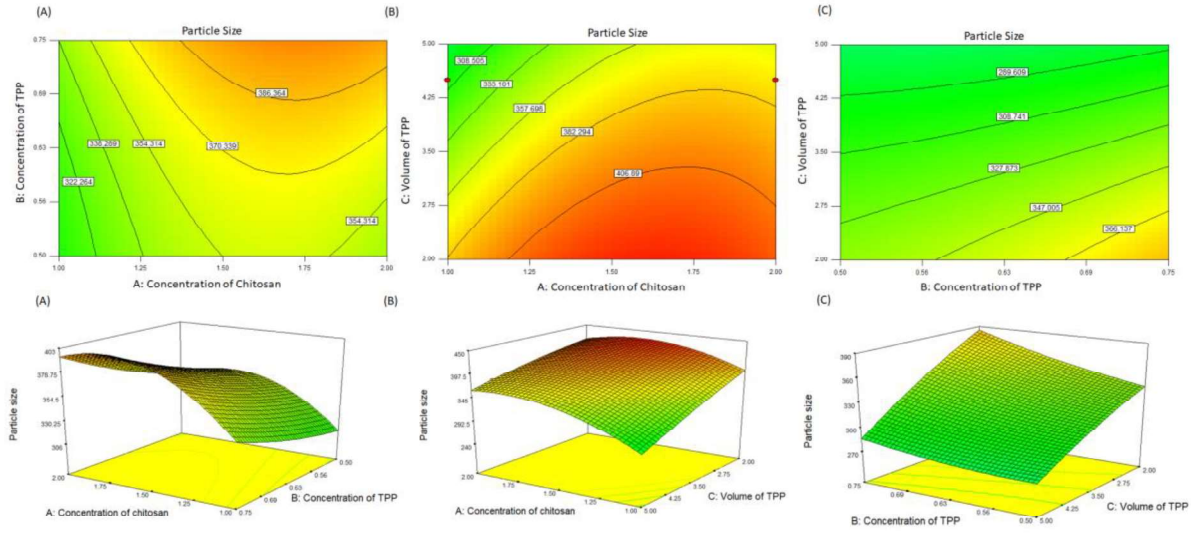

Figure 3.5 2D Contour plot (A,B,C) and 3D response surface (A,B,C) showing effect of different factors like concentration of chitosan and TPP on particle size of nanoparticles.

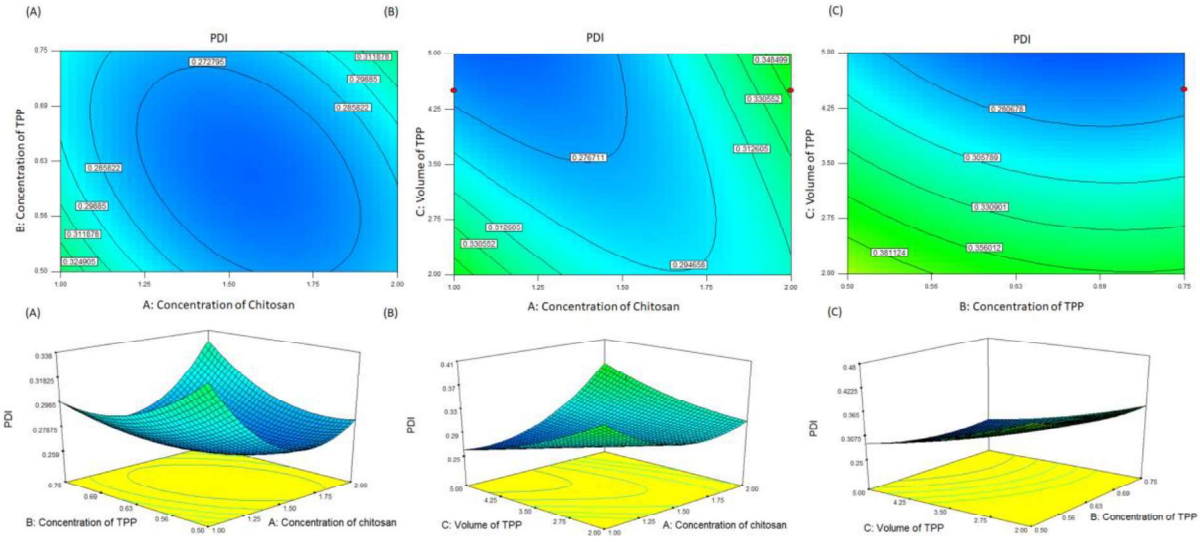

Figure 3.6 2D Contour plot (A,B,C) and 3D response surface (A,B,C) showing effect of different factors like concentration of chitosan and TPP on particle size distribution of nanoparticles.

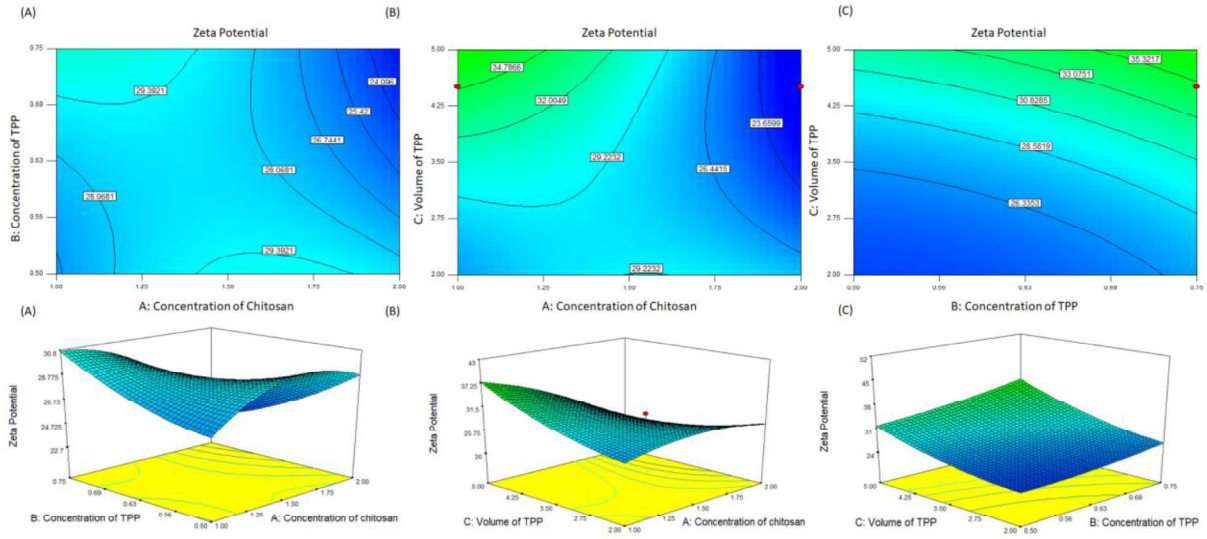

Figure 3.7 2D Contour plot (A,B,C) and 3D response surface (A,B,C) showing effect of different factors like concentration of chitosan and TPP on zeta potential of nanoparticles.

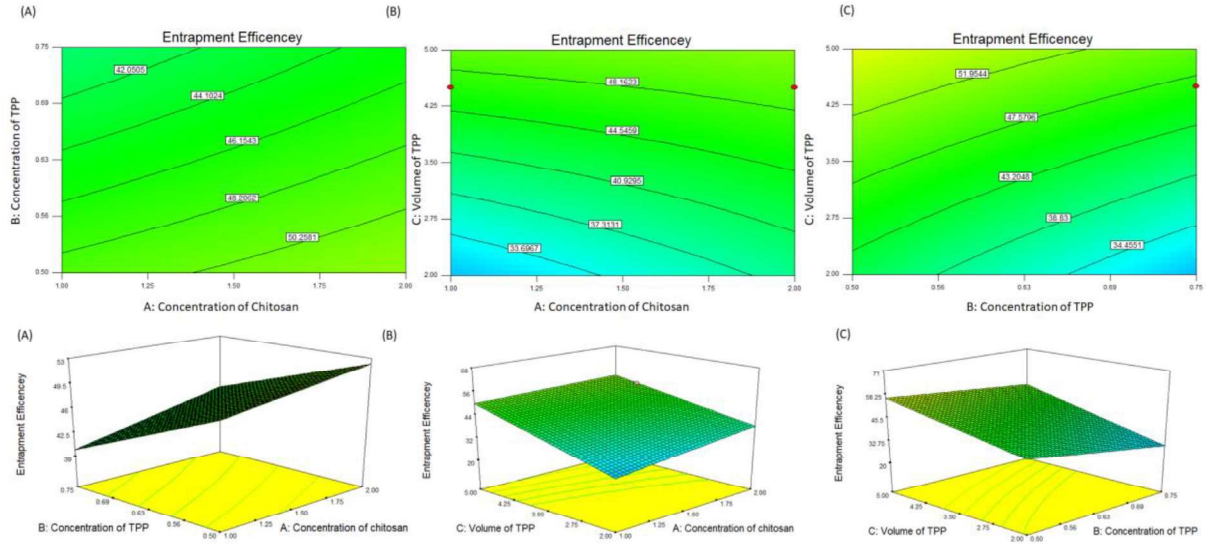

Figure 3.8 2D Contour plot (A,B,C) and 3D response surface (A,B,C) showing effect of different factors like concentration of chitosan and TPP on entrapment efficiency of nanoparticles.

3.5.3 Optimization and validation of nanoformulations

GMC-CSN-NPs were prepared with the objective of keeping the particle size and PDI minimum, zeta potential and percent entrapment efficiency maximum. The optimized batch of nanoparticles was prepared using 1mg/ml of CSN, 0.5 mg/ml of TPP and 8 ml volume of TPP solution. The optimised composition was used to prepare GMC-CSN-NPs. The Adeq Precision" measures the signal to noise ratio, a ratio greater than 4 is desirable. Particle size, PDI, zeta potential, and entrapment efficiency values for the optimised batch indicated that the obtained values were in good correlation with the

predicted values **(Table 3.7).** The optimized formulations were used further for *in vitro* and *in vivo* experiments.

Table 3.7 Physicochemical characterization of optimized chitosan nanoparticles.

Type of Formulation	Particle size (nm)	PDI	Zeta potential (mV)	Entrapment efficiency (%)
Optimized NPs	152.11	0.236	54.35	70.52
Obtained NPs	148.56±8.46	0.248±0.011	51.97±2.30	72.24±2.56

3.5.4 Characterization of chitosan nanoparticles and 5-N-acetyl-neuraminic acid conjugated chitosan nanoparticles

3.5.4.1 Characterization of CSN-Neu5Ac conjugate

The purified CSN-Neu5Ac conjugate was characterized by ^{1}H NMR spectroscopy to authenticate the conjugation and assess product purity. Finally, HR-MS and FTIR analysis was used to confirm the identification of the CSN-Neu5Ac conjugate.

3.5.4.1.1 NMR

The formation of CSN-Neu5Ac conjugate was confirmed by ^{1}H NMR spectra (Bruker BioSpin International AG). The CSN-Neu5Ac conjugate was formed due to formation of an amide linkage between the active N-Hydroxysuccinimide ester of Neu5Ac and the primary amine group of CSN. The spectra of CSN-Neu5Ac conjugate showed two characteristic peaks of N-H bond along with amide bond. The peak for one N-H hydrogen in R-(CO)-N-H was detected at 8.09 ppm whereas the peak for another hydrogen connected to nitrogen in CH_3-(CO)-N-H was detected at 8.10 ppm. Moreover, both these peaks were missing from the CSN-Neu5Ac conjugate's D2O exchange NMR spectrum **(Figure 3.9 A, B & C).**

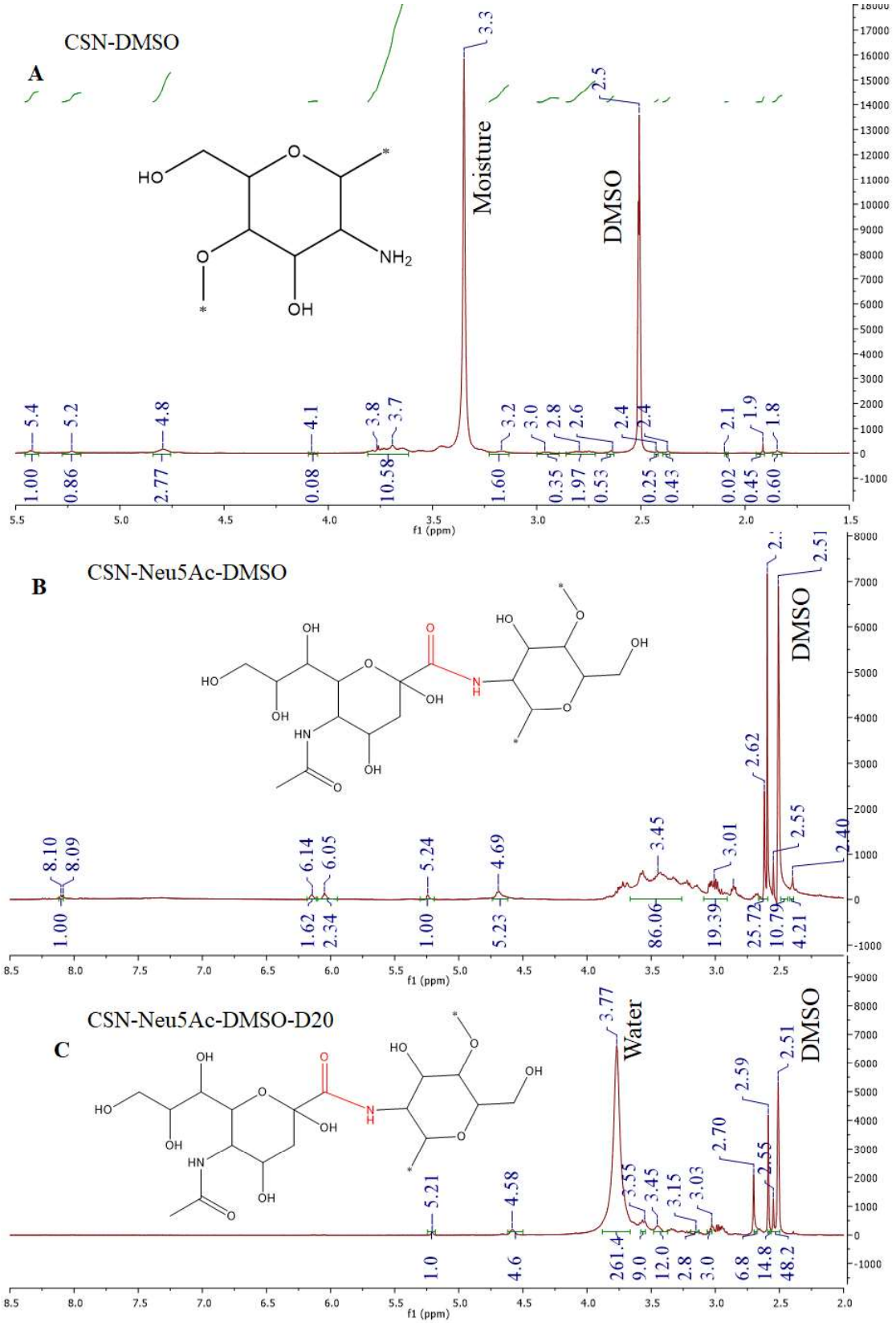

Figure 3.9 [1]H NMR spectra of: A. chitosan (CSN) in DMSO B. chitosan-5-N-acetyl-neuraminic-acid (CSN-Neu5Ac) conjugate in DMSO C. chitosan-5-N-acetyl-neuraminic-acid (CSN-Neu5Ac) conjugate D2O exchange.

3.5.4.1.2 Mass spectroscopy

HR-MS analysis **(Figure 3.10)** was further used to confirm the formation of CSN-Neu5Ac conjugate. The molecular ion peak in the MS spectra of chitosan was observed at *m/z* 1528. A prominent peak of Neu5Ac in the MS spectra operating in positive ionisation mode was recorded at m/z 309.27, corresponding to the m+1 molecular weight, which was observed at m/z 310.11. The peak assigned at *m/z* 1819.13 confirmed CSN-Neu5Ac conjugation. Additionally, peaks obtained at *m/z* 1818.77 and *m/z* 1819.35, were linked to isotopic variants of the conjugate.

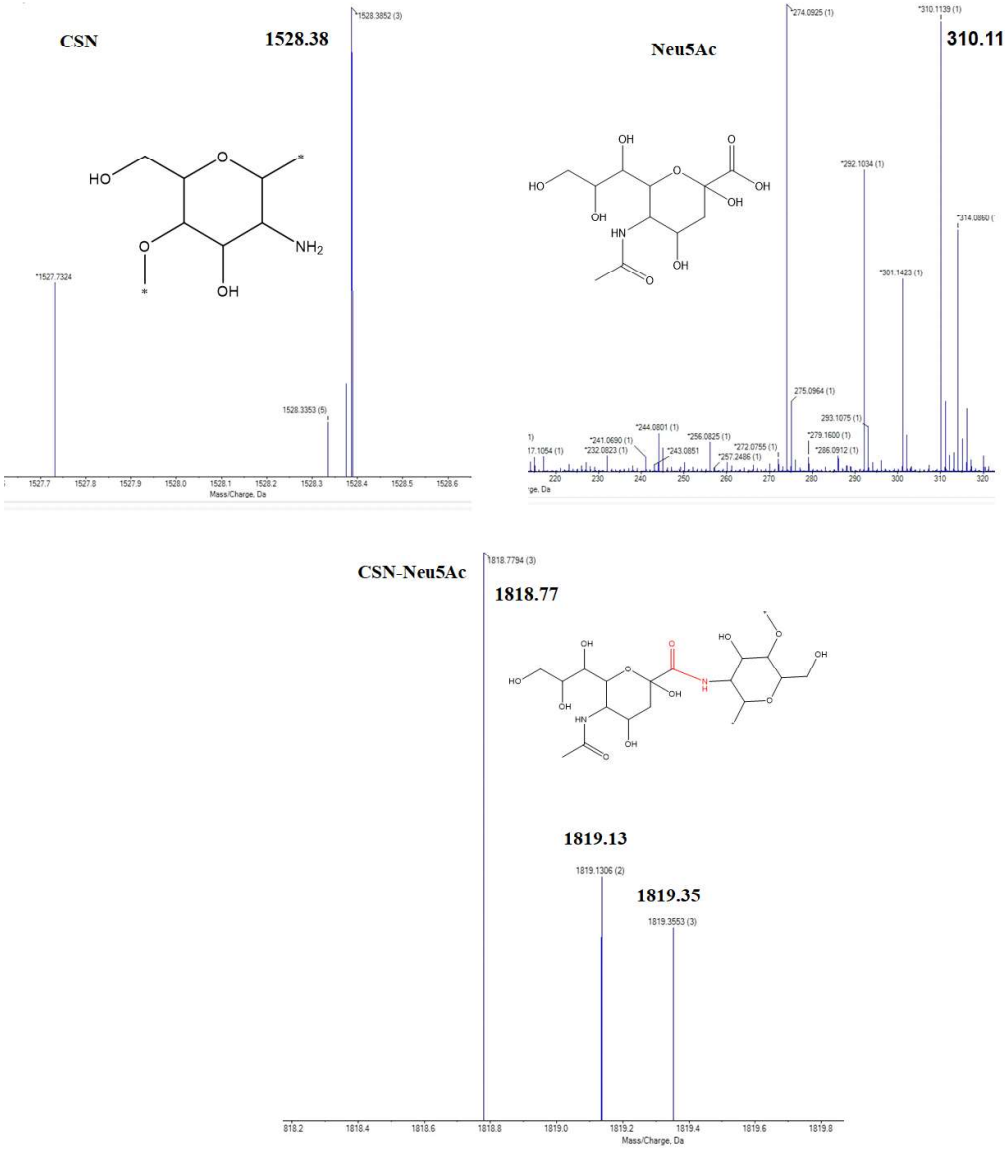

Figure 3.10 HRMS spectra of chitosan (CSN), 5-N-acetyl-neuraminic-acid (Neu5Ac) and chitosan-5-N-acetyl-neuraminic acid (CSN-Neu5Ac) conjugate.

3.5.4.1.3 Fourier transform infrared (FTIR) spectroscopy

The CSN FTIR spectra **(Figure 3.11)** showed a broad absorption band at 3450 cm^{-1}, which was attributed to intermolecular hydrogen bonding between O-H and N-H bands. The peaks adjacent to 2910, 1158, 1080 and 890 cm^{-1} resulted from the stretching vibrations of aliphatic C-H, C-O, C-O-C and C-C bonds respectively. CSN showed C-N stretch at 1380 cm^{-1} and N-H bending at 1628 cm^{-1} which was due to free amine groups in CSN. The Neu5Ac FTIR spectra showed characteristic absorption bands at 1723 and 1652 cm^{-1}, which represented the stretching vibration of the carbonyl group (C=O) in carboxyl (-COOH) and amide (-CONH) groups, respectively. The CSN-Neu5Ac FTIR spectrum displayed an obvious increase in the intensity of the absorption band at 3411 cm^{-1} due to overlapping of peaks of O-H and N-H functional groups. In Neu5Ac, the intensity of the stretching of carbonyl group in -CONH decreased and slightly shifted from 1652 to 1634 cm^{-1}. Simultaneously, the absorption bands at 1723 cm^{-1} and 1628 cm^{-1} derived from carbonyl group at the carboxyl groups of Neu5Ac and amine group of CSN respectively disappeared. However, new peak appeared at 1563 cm^{-1} which could be due to formation of secondary amide bond (-CONH) along with a newly formed peak at 1706 cm^{-1} due to C=O stretching vibration confirming the conjugation of Neu5Ac and CSN.

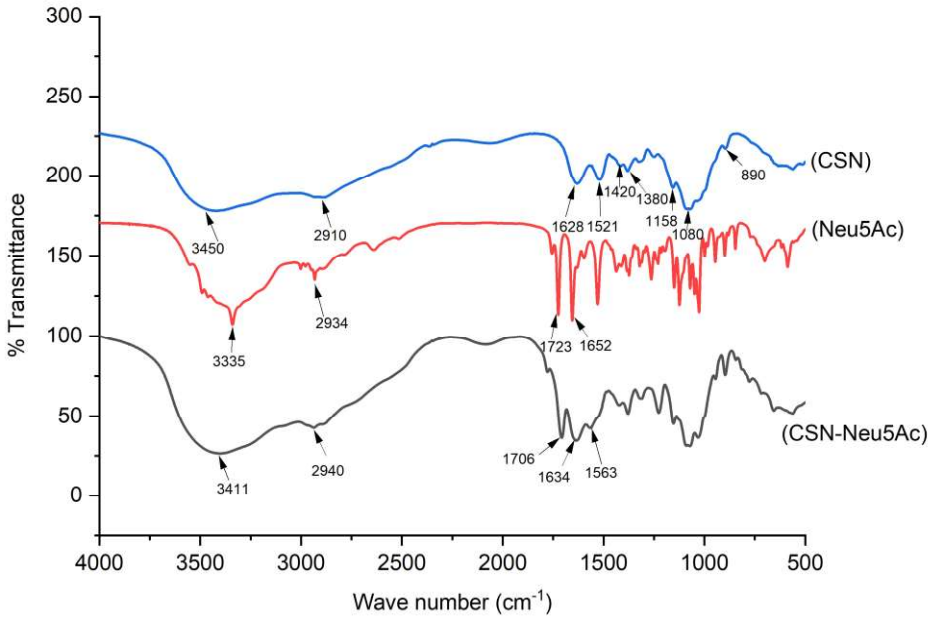

Figure 3.11 FTIR spectra of chitosan (CSN), 5-N-acetyl-neuraminic-acid (Neu5Ac) and chitosan-5-N-acetyl-neuraminic-acid (CSN-Neu5Ac) conjugate.

3.5.4.2 Physiochemical characterization of nanoparticles

Transmission electron micrographs demonstrated uniform and spherical morphology of GMC-CSN-NPs and GMC-CSN-Neu5Ac-NPs. The TEM images of GMC-Neu5Ac-CSN-NPs showed larger size particles compared to GMC-CSN-NPs may be due to conjugation of targeting ligand, Neu5Ac. Scanning electron micrographs of all GMC encapsulated CSN-NPs showed smooth surface topography with almost spherical texture and mono-disperse particle size distribution.

The atomic force microscopy (AFM) was performed in semi-contact 2-D and 3-D mode under high vacuum to identify surface morphology of GMC-CSN-NPs, and GMC-CSN-Neu5Ac-NPs. Roughness, height and morphological features of NPs were evaluated in AFM. Spherical particles with smooth surface were observed and in comparison with GMC-CSN-NPs, the GMC-CSN-Neu5Ac-NPs exhibited higher height, probably due to the presence of Neu5Ac over the surface of CSN-NPs **(Figure 3.12).**

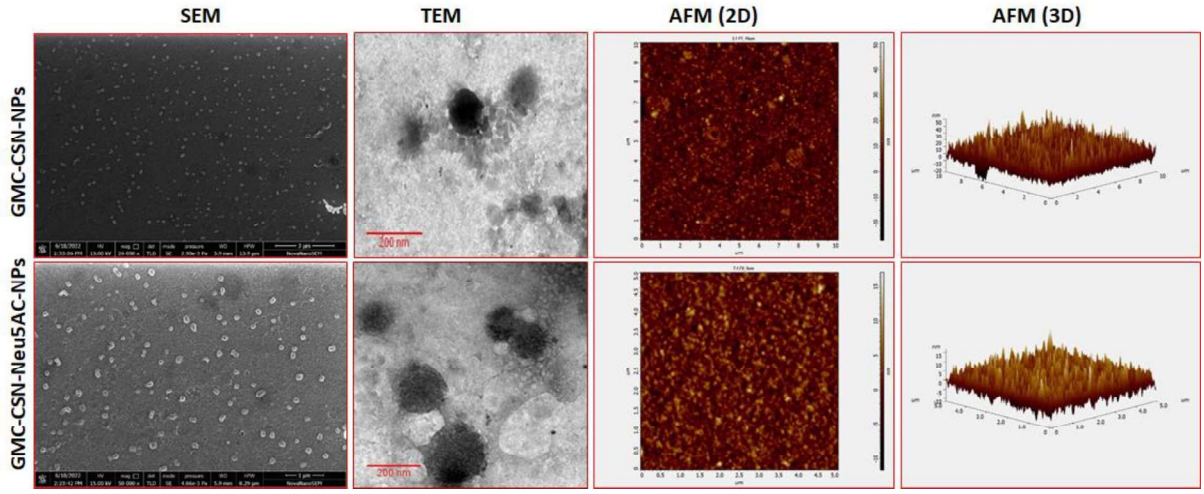

Figure 3.12 Morphological characterization of non-targeted (GMC-CSN-NPs) and glycan receptor targeted (GMC-CSN-Neu5Ac-NPs) nanoparticles.

The size and distribution of NPs are critical parameters for the drug carrier system as NPs typically distribute throughout the body in size-dependent fashion [241]. The targeted and non-targeted CSN-NPs nanoparticles exhibited hydrodynamic particle diameter approximately in the range of 140 to 170 nanometres (nm). The particle size of glycan receptor targeted CSN-NPs (GMC-CSN-Neu5Ac-NPs) was 161.16±7.70 nm, which was higher than that of non-targeted CSN-NPs (GMC-CSN-NPs)

145.66±5.56 nm may be due to presence of Neu5Ac on the surface of CSN-NPs. The PDI of GMC-CSN-NPs and GMC-CSN-Neu5Ac-NPs was 0.26±0.004 and 0.30±0.01 respectively, in the range of 0.2-0.3, indicating consistently distributed particles. Such nanoparticles are preferably suitable for delivery to cancerous cells [242]. Research has shown that nano-sized particles with less than 200 nm exhibited extended blood circulation time, reticuloendothelial system (RES) escape, and high accumulation at cancerous sites *in vivo* via enhanced permeation and retention (EPR) effect [5,243].

The zeta potential of GMC-CSN-NPs and GMC-CSN-Neu5Ac-NPs was found to be 50.66±3.74 mV and 40.3±3.45 mV respectively, indicating formation of highly stable formulation. It was observed that the surface charge of GMC-CSN-Neu5Ac-NPs decreased, probably due to surface modification of cationic charge in CSN-NPs by Neu5Ac which is negatively charged, further suggesting conjugation of Neu5Ac on the surface of CSN-NPs **(Table 3.8).**

Table 3.8 Physiochemical characteristics of nanoparticles.

Nanoformulation	Particle size (nm) (Mean ± SD)	PDI (Mean ± SD)	Zeta potential (mV) (Mean ± SD)	%EE (Mean ± SD)
GMC-CSN-NPs	145.66±5.56	0.262±0.004	50.66±3.74	70.29±2.18
GMC-CSN-Neu5Ac-NPs	161.16±7.70	0.303±0.011	40.3±3.45	66.11±1.94
DiD-GMC-CSN-NPs	149.2±4.05	0.282±0.019	48.16±1.76	69±2.48
DiD-GMC-CSN-Neu5Ac-NPs	169.46±7.08	0.309±0.040	40.1±2.86	66.27±3.06

XPS was used for surface elemental analysis of GMC-CSN-NPs and GMC-CSN-Neu5Ac-NPs. The presence of characteristic peaks of oxygen, carbon and nitrogen was observed in the XPS spectra of the corresponding nanoparticles (**Figure 3.13 A).** An increase in the atomic percentage of oxygen (O 1s) and nitrogen (N 1s) in the XPS spectra of GMC-CSN-Neu5Ac-NPs was observed **(Table 3.9)** due to presence of Neu5Ac residues on surface of CSN-NPs indicating successful conjugation of Neu5Ac on CSN-NPs.

Table 3.9 Atomic Proportion of O1s, C1s and N1s in GMC-CSN-NPs and GMC-CSN-Neu5Ac-NPs.

S.no	Formulation	Atomic %		
		O1s	C1s	N1s
1.	GMC-CSN-NPs	26.99	65.2	7.81
2.	GMC-CSN-Neu5Ac-NPs	27.28	63.9	8.83

The XRD spectra of the GMC and Neu5Ac displayed distinct sharp peaks due to their crystalline nature. However, broad peaks were observed in the XRD of CSN indicating its amorphous state. The XRD spectra of CSN-Neu5Ac conjugate exhibited distinct broad peaks indicating conjugation of Neu5Ac on the surface of CSN in amorphous form. The XRD spectra of GMC-CSN-NPs and GMC-CSN-Neu5Ac-NPs also showed broad peaks indicating entrapment of GMC in amorphous form within the NPs **(Figure 3.13 B).**

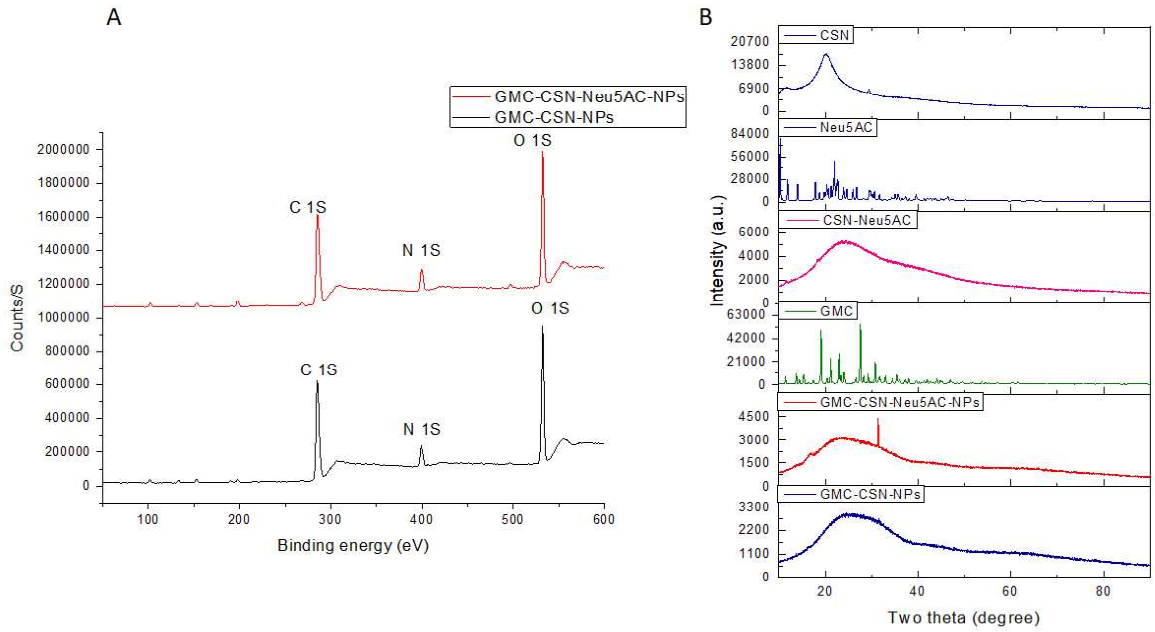

Figure 3.13 (A) XPS spectra of non-targeted (GMC-CSN-NPs) and glycan receptor targeted (GMC-CSN- Neu5Ac-NPs) nanoparticles (B) XRD overlay spectra of CSN, Neu5Ac, CSN-Neu5Ac, GMC-CSN-NPs and GMC-CSN-Neu5Ac-NPs.

3.5.5 Evaluation of Entrapment efficiency and *in vitro* drug release

Entrapment efficiency of GMC loaded non-targeted (GMC-CSN-NPs) and glycan receptor targeted (GMC-CSN-Neu5Ac-NPs) CSN-NPs was calculated as 70.24±2.13 % and 66.11±1.94 % respectively **(Table 3.8).** Targeted nanoparticles exhibit lower entrapment efficiency due to steric hindrance by surface conjugation of Neu5Ac residues on the surface of CSN-NPs [244].

Drug release from the nanoparticles is a prerequisite to desirable therapeutic effect. The release of GMC from CSN-NPs was analysed by dialysis bag diffusion method at two different pH values: in acetate buffer with pH 5.5 simulating cancer microenvironment and PBS at pH 7.4 mimicking the

physiological condition. The cumulative percentage release of GMC from CSN-NPs after 72 h was nearly 90.83± 1.30 % (GMC-CSN-NPs) and 87.56± 2.13 % (GMC-CSN-Neu5Ac-NPs) at pH 5.5, 58.51±3.74 % (GMC-CSN-NPs) and 51.50±2.44 % (GMC-CSN-Neu5Ac-NPs) at pH 7.4. The cumulative GMC release v/s time interval plot shows that GMC-CSN-NPs and GMC-CSN-Neu5Ac-NPs manifest a biphasic drug release pattern **(Figure 3.14)** from polymeric matrix of CSN-NPs and CSN- Neu5Ac-NPs [245]. A similar pattern of initial burst release, followed by sustained drug release was observed in both acetate (pH 5.5) and PBS (pH 7.4) buffer. The release of GMC from CSN-NPs at pH 5.5 was faster as compared to that at pH 7.4. This quicker release at low pH value (pH 5.5) may be due to higher solubility of CSN in acidic pH that results in leakage of GMC from CSN-NPs. It follows that GMC-CSN-NPs and GMC-CSN-Neu5Ac-NPs could exhibit pH sensitive release of encapsulated GMC *in vivo* and, consequently, provide greater GMC accumulation intracellularly in cancer interstitium.

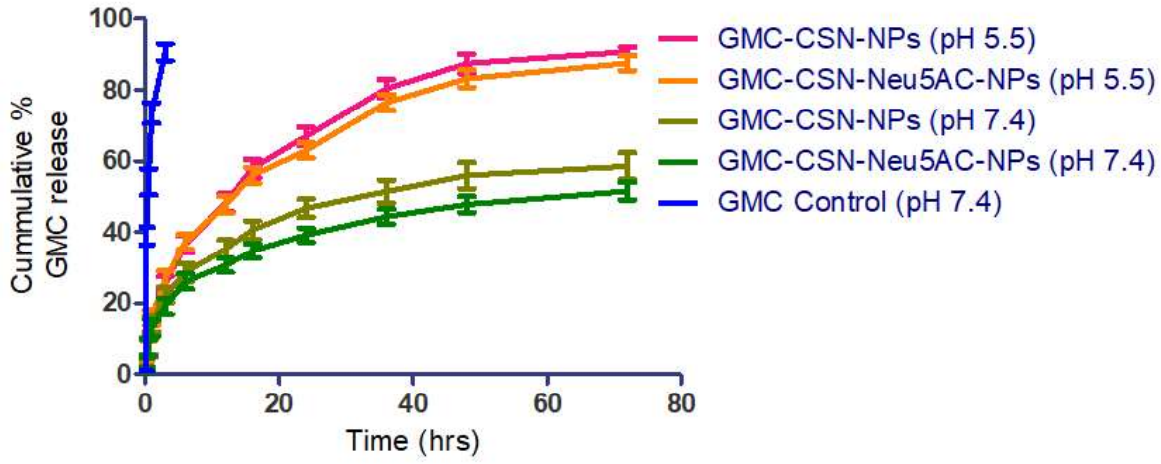

Figure 3.14 *In vitro* release of GMC from non-targeted (GMC-CSN-NPs) and glycan receptor targeted (GMC-CSN- Neu5Ac-NPs) nanoparticles in acetate buffer (pH 5.5) and PBS buffer (pH 7.4).

3.5.6 Cellular uptake analysis

The blue fluorescence shown by DAPI-stained nuclei was surrounded by the green fluorescence of C6 labelled GMC-CSN-NPs and GMC-CSN-Neu5Ac-NPs indicating that a large fraction of the NPs may be embedded into the cytoplasm (**Figure 3.15 A)**. The cellular uptake of targeted GMC-CSN-Neu5Ac-NPs was compared to non-targeted GMC-CSN-NPs and GMC control by measuring the total

area occupied by green fluorescent images (fluorescent intensity) due to C6 using image-J software. The total area occupied by green fluorescent images of C6 tagged GMC control, GMC-CSN-NPs and GMC-CSN-Neu5Ac-NPs was 0.45±0.15, 0.89±0.20 and 1.91±0.10. The total area covered by C6 was non-significantly ($p > 0.05$) different with GMC control than non-targeted NPs (GMC-CSN-NPs) but significantly higher ($p < 0.001$) with glycan receptor targeted NPs (GMC-CSN-Neu5Ac-NPs) than GMC control and non-targeted NPs (GMC-CSN-NPs) (**Figure 3.15 B)**. These findings suggested that glycan receptor-targeted CSN-NPs gradually increased cellular uptake in A-549 cells, demonstrating the importance of receptor-mediated endocytosis. Green fluorescence intensity was more intense and uniformly distributed across the entire cytoplasm with GMC-CSN-Neu5Ac-NPs as compared to GMC-CSN-NPs and GMC control. The study suggest that glycan receptor targeted nanoparticles (GMC-CSN-Neu5Ac-NPs) enter and concentrate in the cells, exhibiting higher cellular uptake.

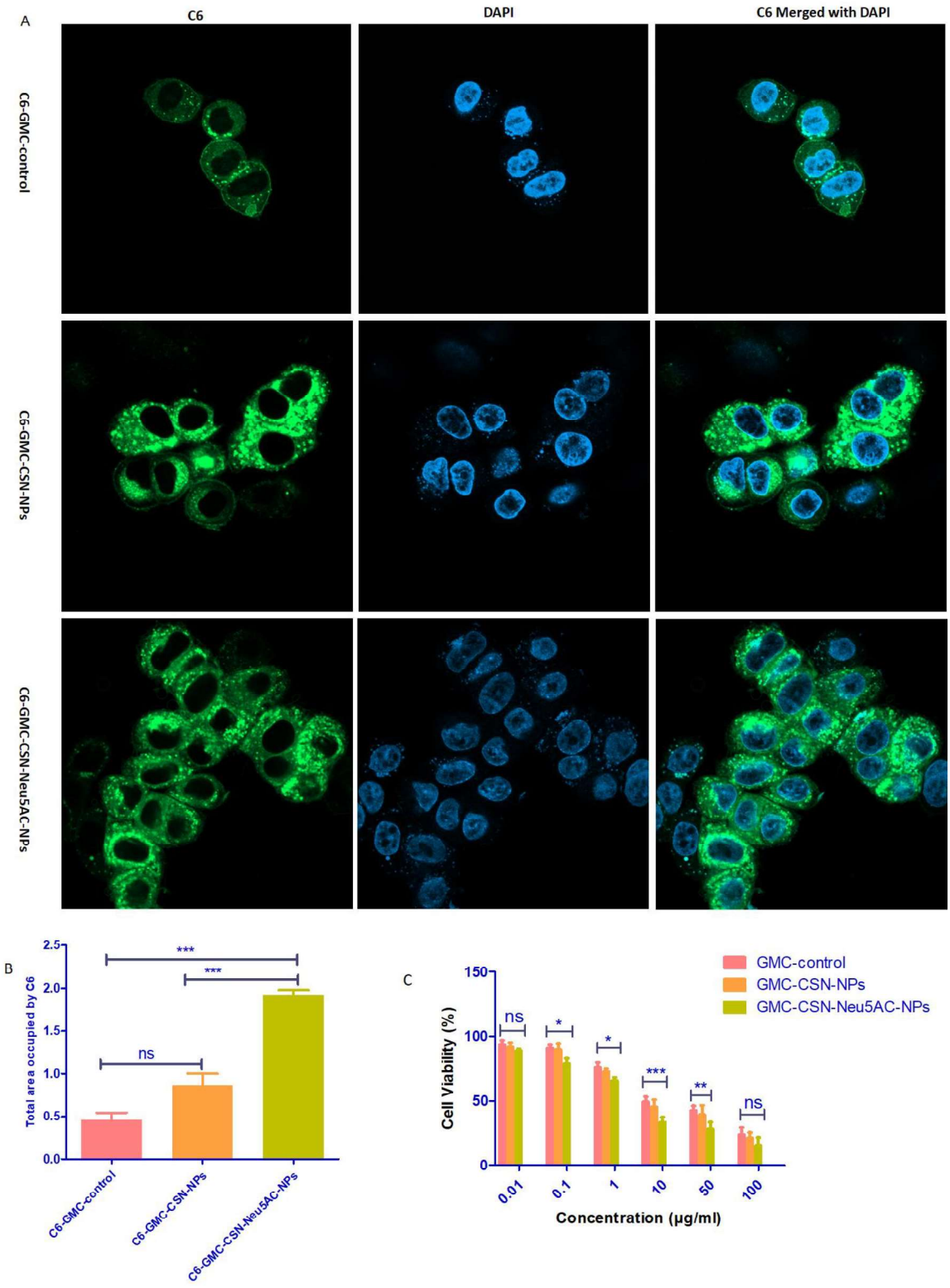

Figure 3.15 (A) A-549 cells showing the cellular uptake of coumarin-6 (C6) tagged GMC control, non-targeted NPs (GMC-CSN-NPs), and glycan receptor targeted NPs (GMC-CSN-Neu5Ac-NPs). (B) Total area covered by C6 (shown by green fluorescent channel) in A-549 lung cancerous cells by GMC control, non-targeted NPs (GMC-CSN-NPs), and glycan receptor targeted NPs (GMC-CSN-Neu5Ac-NPs) was examined by Image-J software (C) % Cell viability of GMC control, non-targeted NPs (GMC-CSN-NPs), and glycan receptor targeted NPs (GMC-CSN-Neu5Ac-NPs). (* $p < 0.05$), (** $p < 0.01$), (*** $p < 0.001$) are statistically significant and ($p > 0.05$) non-significant (ns).

3.5.7 Cytotoxicity study

The percent cell viability of glycan receptor targeted NPs (GMC-CSN-Neu5Ac-NPs) was lower than that of non-targeted NPs (GMC-CSN-NPs) and GMC control respectively (**Figure 3.15 C)**. The IC50 value indicates the chemotherapeutic effect of nanoformulation as a measure of cytotoxicity. After 24 h of exposure of A-549 cells, the IC50 values of GMC control, GMC-CSN-NPs, and GMC-CSN-Neu5Ac-NPs were 16.52±2.05 µg/ml, 10.15±2.66 µg/ml and 6.39±3.78 µg/ml respectively. It can thus be inferred that with increase in drug concentration from 0.01 µg/ml to 100 µg/ml of Neu5Ac decorated CSN-NPs, there was increase in cytotoxicity of Neu5Ac binding (glycan) receptor in lung cancer A-549 cells. This might be due the result of enhanced cellular uptake and delivery of GMC to cancerous cells through receptor-mediated endocytosis of targeted nanoparticles. These findings indicate that glycan receptor targeted chitosan nanoparticles (GMC-CSN-Neu5Ac-NPs) dramatically increased the anti-proliferative effect of GMC on A-549 cells.

3.5.8 Tissue bio-distribution study

The quantity of drug estimated in particular organs upon delivery of GMC-CSN-NPs and GMC-CSN-Neu5Ac-NPs has been shown in **(Figure 3.16)**. Significantly high amount of GMC was measured in lung cancerous tissues along with some traces in hepatic and renal tissues, upon administration of GMC-CSN-Neu5Ac-NPs compared with GMC-CSN-NPs and GMC control. The amount of GMC in lung cancerous tissues delivered through GMC-CSN-Neu5Ac-NPs was approximately17.42 ± 1.35 % after 2 h, which increased to 34.09 ± 2.45 % at 12 h and was maintained at 13.63±1.77 % beyond 24 h probably due to sustained release of drug. The amount of GMC estimated in hepatic and renal tissues was relatively smaller in comparison to lungs with very minor amount being present in heart and spleen indicating targeted delivery of GMC-CSN-Neu5Ac-NPs and can be expected to bring down the drug associated cell toxicity. 12.47 ± 2.03 %, 10.59 ± 1.24 % and 3.27 ± 1.44 % GMC was released from GMC-CSN-NPs at 2 h, 12 h and 24 h respectively, whereas almost negligible concentration of GMC was found after 2 h upon administration of free drug solution. These results revealed that GMC-CSN-Neu5Ac-NPs have better lung cancer targeting ability due to presence of targeting ligand 5-N-acetyl-neuraminic acid.

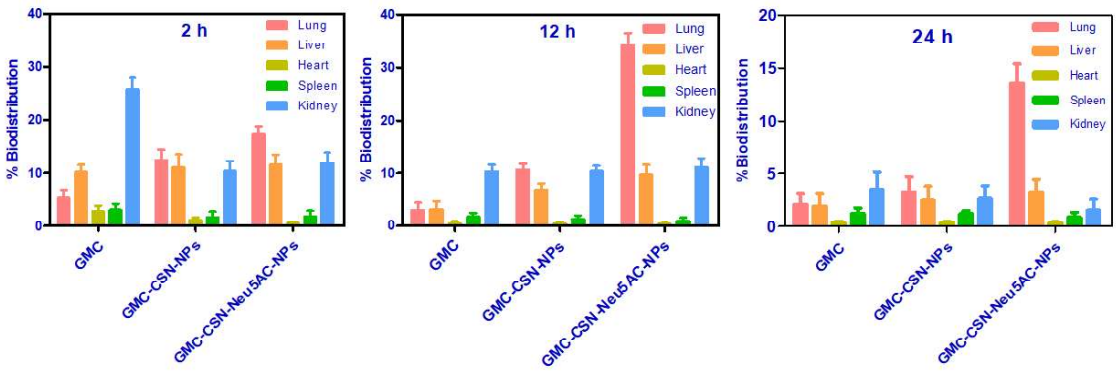

Figure 3.16 Tissue bio-distribution of GMC control, GMC-CSN-NPs and GMC-CSN-Neu5Ac-NPs at different time points; the data has been presented as mean ± SD (n=3).

3.5.9 *In vivo* fluorescent bio-imaging

The real-time bio-distribution and targeting efficacy of CSN-NPs in swiss albino mice was assessed through *in vivo* fluorescent imaging **(Figure 3.17 A).** The bio-images showed that DiD-GMC-CSN-Neu5Ac-NPs distributed progressively and showed higher accumulation in cancerous region upon intravenous administration. Higher intensities of fluorescence signals of DiD-GMC-CSN-Neu5Ac-NPs were measured in comparison to that of DiD-GMC-CSN-NPs in the lung tissues at 24 h. While DiD distributed rapidly and non-specifically in cancerous tissue, with the fluorescence signal being highest at 1 h, a steady decline in the intensity was observed up to 12 h, with no signal being observed after 24 h. As DiD-GMC-CSN-Neu5Ac-NPs exhibited considerably higher fluorescence intensity at the cancerous site than DiD-GMC-CSN-NPs and DiD, it implies the potential of Neu5Ac conjugated CSN-NPs to efficiently deliver GMC into the cancerous region and be retained there for extended period of time. The targeting efficiency of conjugated NPs was further confirmed by *ex vivo* fluorescence imaging. *Ex vivo* images **(Figure 3.17 B)** of extracted organs 24 h post injection of DiD-GMC-CSN-Neu5Ac-NPs clearly displayed strong fluorescence signal in lungs, but there was weak signal of DiD-GMC-CSN-NPs and no visible signal from free DiD in lungs. However, DiD-GMC-CSN-NPs showed strong signal of DiD in liver indicating non-specific distribution of these NPs. DiD-GMC-CSN-NPs and DiD were distributed systemically in the body via biological membranes following passive diffusion mechanism and molecular phagocytosis that resulted in their poor transport to lung cancerous regions. However, DiD-GMC-CSN-Neu5Ac-NPs exhibited sustained

effect and escaped phagocytosis, resulting in higher availability of nanoparticles in cancerous tissues probably via receptor-mediated endocytosis due to binding of Neu5Ac to glycan receptors [246].

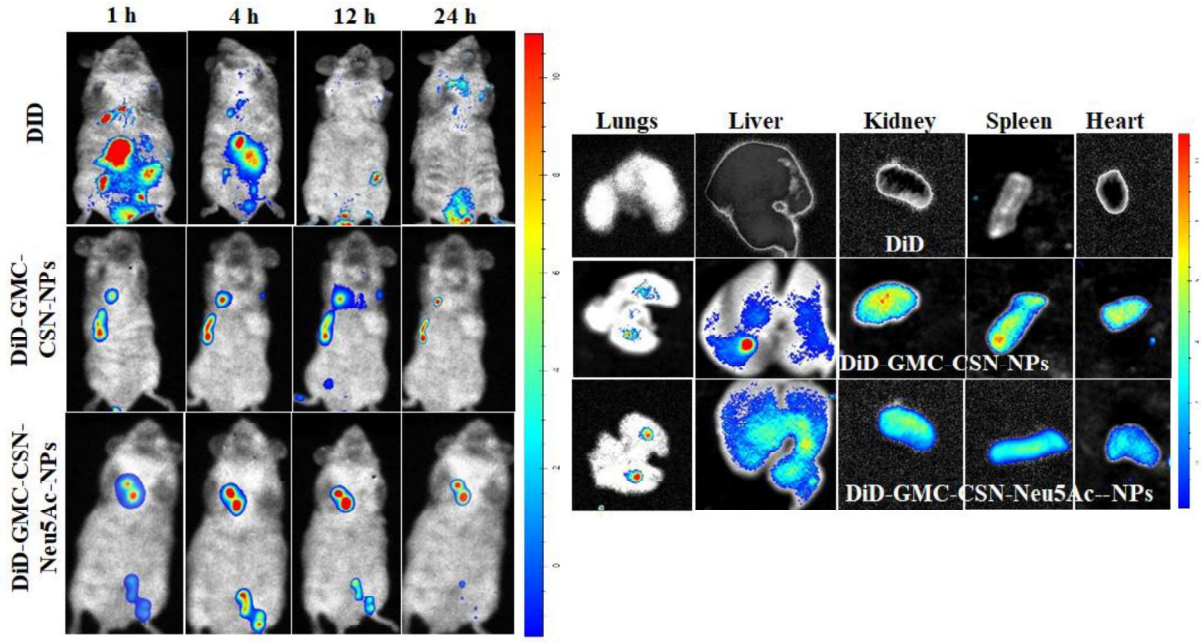

Figure 3.17 (A) Optical *In vivo* fluorescent imaging of DiD dye, targeted and non-targeted CSN-NPs (indicted by red fluorescence) in swiss albino mice. (B) *Ex vivo* fluorescence images of organs in lung cancer-bearing mice 24 h post-injection of free DiD, DiD-GMC-CSN-NPs and DiD-GMC-CSN-Neu5Ac-NPs. IVIS images showing higher tissue accumulation of DiD dye-labelled GMC-CSN-Neu5Ac-NPs as compared to GMC-CSN-NPs at 24 h after IV administration into mice bearing lung adenocarcinoma.

3.5.10 Histopathological Observation

The tissue samples of GMC-CSN-NPS and GMC-CSN-Neu5Ac-NPs treated groups were collected and examined and compared with GMC and untreated saline control groups **(Figure 3.18).** Normal bronchial and alveolar epithelial tissues, normal mild inflammatory infiltrates (lungs), normal hepatocytes (Liver), normal glomerulus with tubules (kidney), and normal cardiomyocytes and connective tissues (Heart) were observed in saline control group animals. GMC control showed diffused interstitial alveoli with pneumocytes, hepatic cell inflammation with mild inflammatory infiltrates, abnormal renal tubular endothelial vasculature and loose cardiomyocytes. GMC-CSN-NPs treated animals showed mild hepatic, renal and cardiac necrotic lesions. H&E stained organs such as the lung, liver, kidney and heart in the GMC-CSN-Neu5Ac-NPs treated groups demonstrated nearly intact physiological structures similar to that of saline control group. It can be suggested that GMC-

CSN- Neu5Ac-NPs can help in significant recovery in the physiological architecture upon intravenous administration in diseased animals.

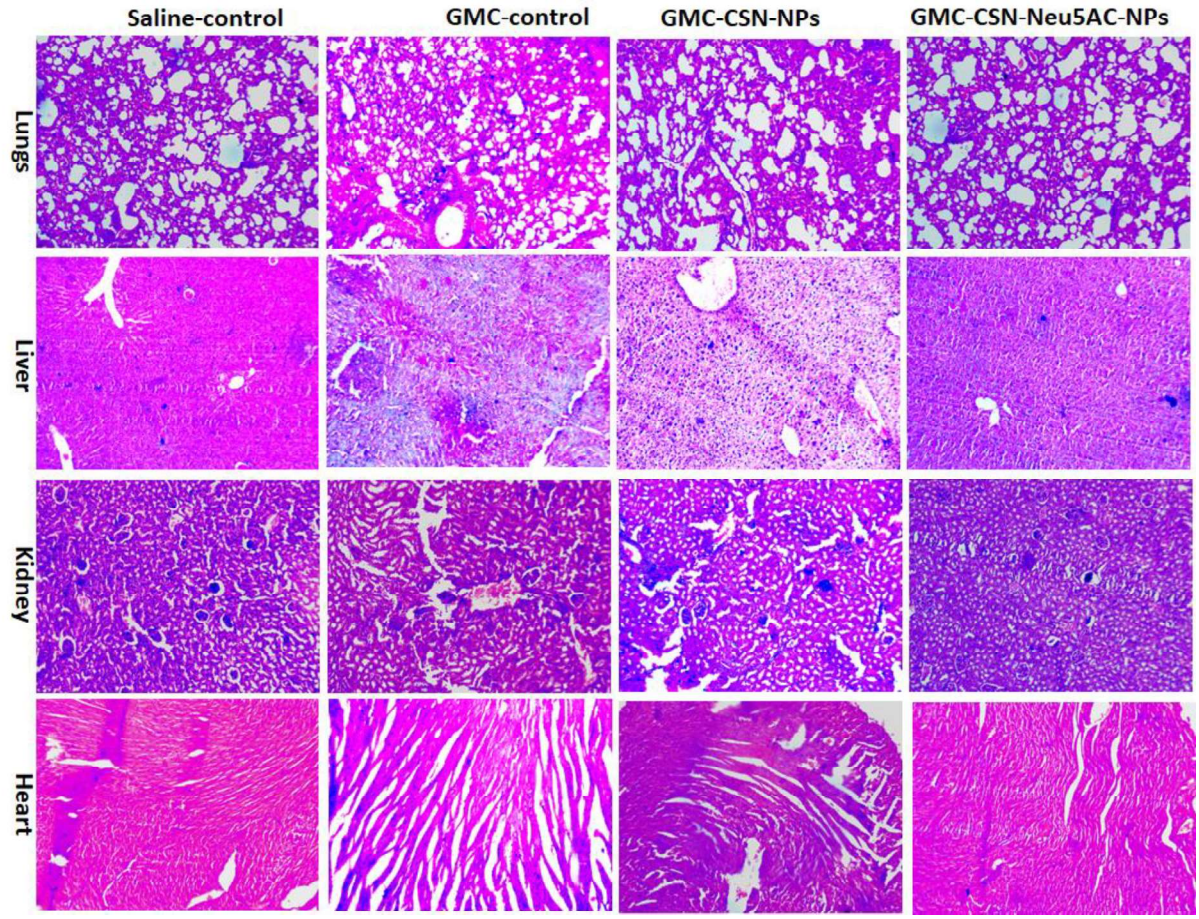

Figure 3.18 H&E stained sections of lungs, liver, kidney and hearts tissues separated from swiss albino mice in various treatment groups: untreated saline control, GMC control, GMC-CSN-NPs and GMC-CSN-Neu5Ac-NPs.

3.5.11 Induction of Lung cancer

Predominantly, cancerous lesions in huge number were noticed in lungs extracted from animals in positive control group, while negative control lungs displayed normal physiological structures **(Figure 3.19 A).** Further, histopathological study confirmed the induction of cancer. In negative control group a normal layer of alveolar epithelial tissue was observed, whereas, positive control group displayed epithelial adenomatous hyperplasia (grey arrow), infiltrating inflammatory cell (blue arrow) and haemorrhage (red arrow) suggesting the formation of pre-malignant and malignant lesions in lung tissues **(Figure 3.19 B).**

3.5.12 *In vivo* anticancer efficacy

The number of cancerous cells in the positive control group was significantly higher *($p < 0.001$)* as compared to negative control. GMC-CSN-NPs and GMC-CSN-Neu5Ac-NPs treated groups showed 1.38 and 2.10-fold decline in the number of metastatic lung epithelial cells, as compared to untreated positive control group *($p < 0.05$)* and *($p < 0.001$)* respectively confirming higher efficacy of the GMC-CSN-Neu5Ac-NPs **(Figure 3.19 C**). While GMC-control group showed non-significant reduction *($p > 0.05$)* in number of metastatic lung epithelial cells as compared to untreated positive control group. Additionally, compared to GMC-CSN-NPs, the GMC-CSN-Neu5Ac-NPs-treated group exhibited higher improvement in the histopathologically observed signs of cancerous transformation. Moreover, GMC-CSN-Neu5Ac-NPs exhibited better anticancer efficacy according to Kaplan-Meier survival analysis, GMC-CSN-Neu5Ac-NPs exhibited comparably better survival rate than GMC-CSN-NPs, because of targeting ability of GMC-CSN-Neu5Ac-NPs which decreased the *in vivo* toxic effects of GMC in normal tissues as compared to GMC-CSN-NPs. **(Figure 3.19 D).** Lungs excised from GMC-CSN-Neu5Ac-NPs treated animals showed significant recovery of cancerous lesions as compared with GMC-CSN-NPs and GMC control **(Figure 3.19 E).** The results of the study indicated that GMC-CSN-Neu5Ac-NPs had significantly higher cell growth inhibition efficiency as compared to GMC control in the animals.

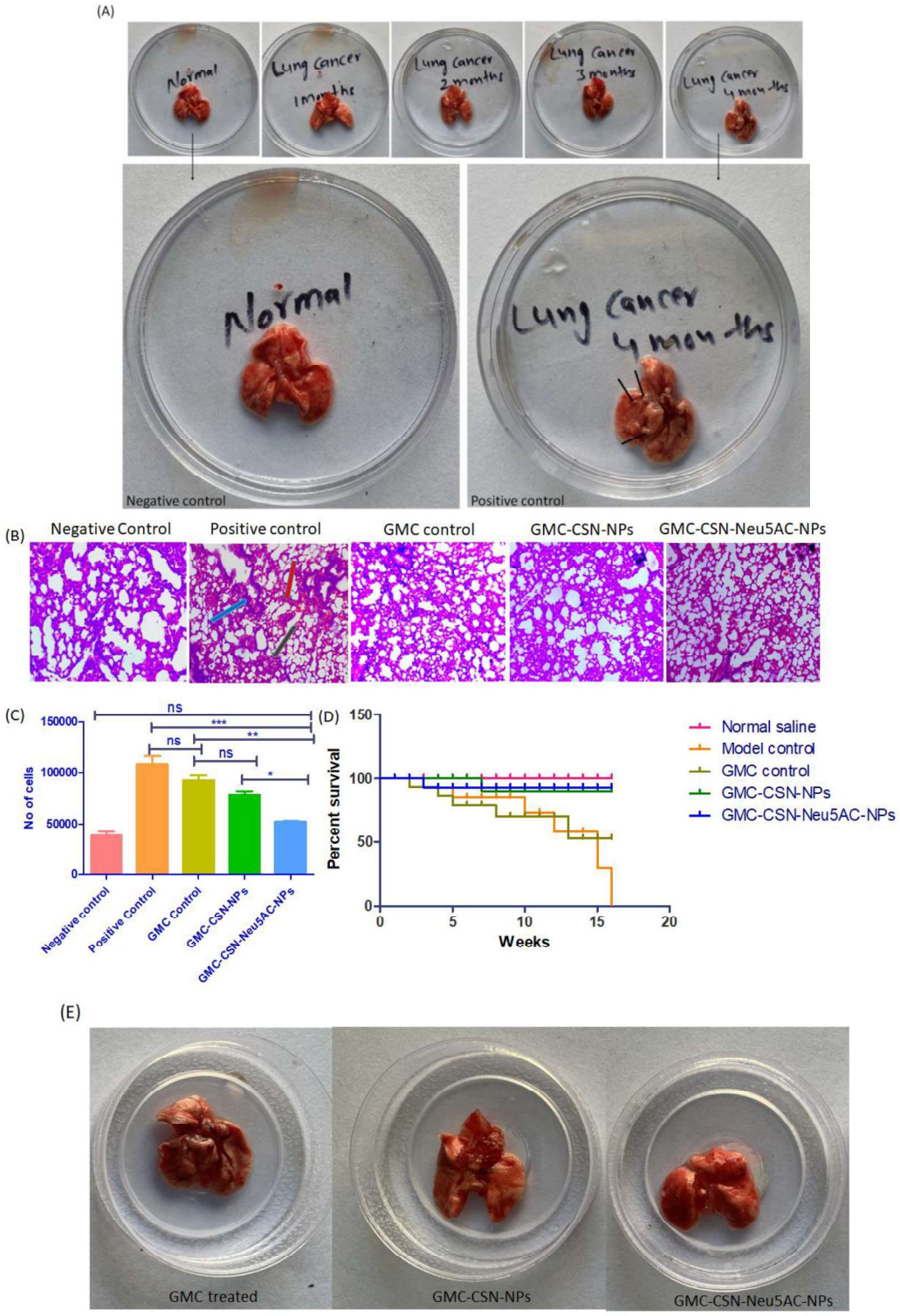

Figure 3.19 (A) Cancerous lesions within 16 weeks of B[a]P treatment in different lungs (positive control); normal group (negative control). (B) Histopathological analysis of H&E stained lung sections of GMC-CSN-NPs and GMC-CSN-Neu5Ac-NPs treatment groups in comparison with untreated diseased positive control and normal negative control group. (C) Number of cells observed in H&E sections of related groups, GMC-CSN-Neu5Ac-NPs: $p > 0.05$ v/s negative control, *** $p < 0.001$ v/s positive control. (D) Kaplan-Meier Survival curve displaying survival of respective treatment groups up to 16 weeks. (E) Comparative visual representation of GMC control, non-targeted and glycan receptor targeted CSN-NPs treated lungs.

3.6 Conclusion

In summary, The CSN-NPs loaded with GMC was successfully optimized by the QBD approach by using least material and resources. The optimization of nanoformulations was done by design of experiments (DoE) utilizing Box Behnken design surface methodology. The optimization of nanoformulations was done with analysis of response, correlation coefficient and desirability approach based numerical optimization technique. Applying this multiple variable statistical design of experiments in the formulations resulted in stable, optimised nanoparticles following an in-depth investigation of the underlying correlation between formulation factors and the expected responses. The ideal range of particle size, PDI, zeta potential and entrapment efficiency were obtained by using a variety of factors specified in design. The optimized formulations were used further for the *in vitro* and *in vivo* experiments. After that a novel encapsulation material was synthesized by conjugation of chitosan with Neu5Ac by carbodiimde chemistry, for targeting glycan receptor in lung cancer. The formation of CSN-Neu5Ac conjugate was confirmed by ^{1}H NMR, HR-MS and FTIR analysis. Then, CSN and Neu5Ac-CSN nanoparticles encapsulated with gemcitabine formulated by ionic cross linking technique. The targeted and non-targeted CSN-NPs nanoparticles exhibited particle sizes less than 200 nm with PDI in the range of 0.2-0.3. The zeta potential (surface charge) of prepared NPs was approximately in the range of +40 to +50 mv indicating high stability. SEM, TEM and AFM analysis demonstrated clear uniform, spherical, smooth regular surface, and monodisperse morphology of CSN-NPs. Surface elemental analysis of CSN-NPs done using XPS also confirmed the successful conjugation of Neu5Ac on CSN-NPs. XRD validated the fact that GMC, though crystalline was entrapped in NP in amorphous form in NPs. The entrapment efficiency of GMC in CSN-NPs was in the range 60-70%. The targeted NPs showed lower entrapment efficiency due to stearic hindrance upon surface conjugation of Neu5Ac residues in CSN-NPs. In addition, CSN-NPs showed ideal drug release behaviour in acidic environment (pH 5.5) which mimics the cancer microenvironment as compared to pH 7.4. The *In vitro* MTT assays and cellular uptake studies revealed anti-proliferation effect and higher cellular uptake by GMC-CSN-Neu5Ac-NPs in A-549 lung cancer cells, indicating the efficiency of targeted therapeutics. The *in vivo* results were analysed in the B[*a*]P induced lung

carcinoma mice model. Tissue bio-distribution studies showed higher lung cancerous tissue accumulation due to active targeting ability of Neu5Ac to glycan receptors, which was further supported qualitatively by bio- imaging studies which showed that Neu5Ac conjugated chitosan nanoparticles exhibited prolonged blood circulation time and realistic targeting ability. Histopathology analysis confirmed the safety of nanoformulations via intravenous administration in lung cancer treatment. Glycan receptor targeted nanoparticles showed significantly higher cancer growth inhibition effect than GMC control in lung cancer mice model. Therefore, GMC loaded Neu5Ac-chitosan nanoparticles targeted to glycan receptor could be potentially developed as an effective therapy for lung cancer therapeutics.